TECHNISCHE UNIVERSITÄT WIEN

DIPLOMARBEIT

Intra- and extracellular stimulation of spiking bipolar cells on macaque's retina

zur Erlangung des akademischen Grades

Diplom-Ingenieurin

im Rahmen des Studiums

Biomedical Engineering

eingereicht von

Sogand Sadat Sajedi
Matrikelnummer 1225220

ausgeführt am Institut für Analysis und Scientific Computing
der Fakultät für Mathematik und Geoinformation der Technischen Universität Wien

Betreuung
Betreuer: Ao.Univ.Prof. Dipl.-Ing. Dr.rer.nat. Dr.sc.med. Dr.techn. Frank Rattay
Mitwirkung: Projektass. Dipl.-Ing. Hassan Bassereh Moosaabadi

Wien, August, 2018

(Unterschrift Verfasser) (Unterschrift Betreuer)

Abstract

Millions of patients are losing their vision all over the world due to retinal degenerative diseases. Losing sight is one of the most debilitating disorders since it severely influences the quality of life and diminishes it. Despite all physical restrictions, lack of this sense results in numerous psychological consequences such as insomnia, social isolation, or even suicidal thoughts. Many worldwide researchers are targeting this group of diseases by using some approaches. For instance, stem cell transplants are one of the promising therapy with many challenges that need to be overcome. Another approach is to replace damaged parts of the retina by engineered living tissues, micro-fabricated photoreceptor arrays, and an implantable electronic micro-system which are referred to as the visual prostheses. The visual prosthesis is designed and developed to either stimulate the nervous system or directly record neural activities with a high spatial resolution.

This study aims to investigate the behaviour of an ON (cone) diffuse bipolar cell DB4 of the macaque retina with intra and extra-stimulations applied and recorded in different parts of the cell. The simulation of the cell is achieved by applying the Hodgkin-Huxley multi-compartment model and employing the Backward Euler solver through Python (Version 2.7). In the end, a channel noise is added to compute more realistic responses and has been compared with the previous results.

Results of the intracellular stimulation show how the electrode position and the waveform is essential in order to get a proper response from the cell. A rectangular pulse is found stronger than a sinusoidal pulse with the same amplitude of 50 pA. The electrode position in sodium band and terminal caused stronger responses in contrast to soma and dendrite. Most spikes are found in frequencies between 20 to 60 HZ.

Results of the extracellular stimulation show that anodic pulses caused stronger stimulation in contrast to cathodic pulses with the same amplitudes specifically in soma, sodium bands and

terminals. The frequency range of the spikes was below 20 Hz. In case of cathodic stimulation more spikes have been found in dendrite with the same frequency range.

According to the root mean square values an adequate k_{noise} for the cell was found in 0.016 $\mu A/(mS)^{1/2}$ which was still not enough to show a stochastic behaviour due to the less sensitivity nature of the bipolar cells. However, after adding the noise, the results show more stochastic structures. In addition to that, stronger responses have been found in the dendrite site of the cell in contrast to the previous responses. Therefore, for further investigations, a more sensitive cell is required to contrast the noise influence in the simulations.

Zusammenfassung

Millionen Patienten verlieren ihre Vision auf der ganzen Erde wegen der Netzhautdegenerativen Erkrankungen. Verlierender Anblick ist eine der schwächende Störungen, da er streng die Lebensqualität beeinflusst und sie vermindert. Trotz aller körperlichen Beschränkungen ergibt Mangel an dieser Richtung zahlreiche psychologische Konsequenzen wie Schlaflosigkeit, Sozialisolierung oder sogar Selbstmordgedanken. Viele weltweiten Forscher untersuchen diese Gruppe Krankheiten an, indem sie einige Ansätze verwenden. Zum Beispiel sind Stammzelletransplantationen eine der viel versprechenden Therapie mit vielen Herausforderungen, die überwunden werden müssen. Eine andere Annäherung ist, geschädigte Teile der Retina durch ausgeführte lebende Gewebe, mikro-fabrizierte Fotorezeptorreihen und ein implantierbares elektronisches Mikrosystem zu ersetzen, die als die visuelle Protheses gekennzeichnet. Die visuelle Protheses wurde entworfen und entwickelt, um entweder das Nervensystem zu stimulieren oder neurale Aktivitäten mit einem hohen räumlichen Bereich direkt aufzuzeichnen Auflösung.

Ziel dieser Studie ist es, das Verhalten einer ON (Zapfen) diffuse bipolaren Zellen DB4 der Makaken-Retina mit Intra- und Extra-Stimulationen zu untersuchen, die in verschiedenen Teilen der Zelle angelegt und aufgezeichnet wurden. Die Simulation der Zelle wird erreicht, indem das Hodgkin-Huxley Multi-Kompartiment Modell und Implizites Euler-Verfahren durch Python (Version 2.7) verwendet wird. Am Ende wird ein Kanalrauschen hinzugefügt, um realistischere Antworten zu berechnen und wurde mit den vorherigen Ergebnissen verglichen.

Die Ergebnisse der intrazellulären Stimulation zeigen, wie die Elektrodenposition und die Wellenform wesentlich sind, um eine korrekte Antwort von der Zelle zu erhalten. Ein rechteckiger Puls wird stärker gefunden als ein sinusförmiger Impuls mit der gleichen Amplitude. Die Elektrodenposition in Natriumband und Terminal verursachte stärkere Reaktionen im Gegensatz zu Dendriten und Soma. Die meisten Spitzen werden in Frequenzen zwischen 20 bis 60 Hz gefunden.

Ergebnisse der extrazellulären Stimulation zeigen, dass anodische Pulse stärkere Stimulation im Gegensatz zu kathodischen Pulsen mit den gleichen Amplituden in Soma, Natriumbanden und terminal verursachen. Der Frequenzbereich der Spikes lag unter 20 Hz. Im Fall der kathodischen Stimulation wurden im Dendriten mit demselben Frequenzbereich mehr Spitzen gefunden.

Entsprechend den quadratischen Mittelwerts wurden für 0,016 $\mu A/(mS)^{1/2}$ ein ausreichendes K_{noise} für die Zelle gefunden, das aufgrund der geringeren Empfindlichkeit der bipolaren Zellen immer noch nicht ausreichte, um ein stochastisches Verhalten zu zeigen. Nachdem Hinzufgen des Rauschens zeigen die Ergebnisse jedoch mehr stochastische Strukturen. Zusätzlich dazu wurden stärkere Antworten in der Dendriten stelle der Zelle im Gegensatz zu den vorherigen Antworten gefunden. Deshalb für weitere Untersuchungen ist daher eine empfindlichere Zelle erforderlich, um den Rauscheinfluss in den Simulationen zu kontrastieren.

List of Abbreviations and Symbols

A	Cross-section of the compartment $[cm^2]$
AC	Amacrine Cell
AIS	Axon Initial Segment
AP	Action Potential
BC	Bipolar Cell
BE	Backward Euler method
C_m	Membrane capacitance $[\mu F/cm^2]$
Ca^{2+}	Calcium ion
Cl^-	Chloride ion
DB	Diffuse Bipolar Cell
DE	Differential Equation
F	Faraday Constant, F=96485.3365 $[C/mol]$
FE	Forward Euler method
g_{Na}	Maximum value of sodium conductance $[mS/cm^2]$
G_{Na}	Sodium conductance $[mS/cm^2]$
g_K	Maximum value of potassium conductance $[mS/cm^2]$
G_K	Potassium conductance $[mS/cm^2]$
g_L	Leak conductance $[mS/cm^2]$
GC	Ganglion Cell

HC	Horizontal Cell
HH	Hodgkin-Huxley model
I	Membrane current $[\mu A/cm^2]$
I_{ax}	Axial current $[\mu A/cm^2]$
I_{ext}	The applied McNeal current
I_{ion}	Ionic current $[\mu A/cm^2]$
I_k	Potassium current $[\mu A/cm^2]$
I_{Na}	Sodium current $[\mu A/cm^2]$
I_{noise}	Noise current $[\mu A/cm^2]$
I_{stim}	Stimulation current $[\mu A/cm^2]$
IPL	Inner Plexiform Layer
K^+	Potassium ion
K_{noise}	Noise factor $[\mu AmS^{-1/2}]$
l	Compartment length [cm]
LTE	Local Truncation Error
M	Axial Matrix
Na^+	Sodium ion
ODE	Ordinary Differential Equation
OPL	Outer Plexiform Layer
P	Probability of gating particles in the open state of a specific ion channel
PR	Photoreceptor cell

r	Radius of the compartment [cm]
R	Gas Constant, R=8.31 $[J/mol.K]$
R_n	Resistance of the compartment $[k\Omega/cm^2]$
RMS	Root Mean Square
T	Temperature [K]
V	Membrane potential [mV]
V_{Na} *or* E_{Na}	Sodium potential [mV]
V_e	Extracellular potential [mV]
V_i	Intracellular potential [mV]
V_k *or* E_k	Potassium potential [mV]
V_L *or* E_L	Leakage potential [mV]
$(X)_e$	Extracellular ion concentration
$(X)_i$	Intracellular ion concentration
α_m,α_n,α_h	Transfer rates from closed to open state [1/ms]
β_m,β_n,β_h	Transfer rates from closed to open state [1/ms]
ρ_{ext}	Extracellular resistivity $[k\Omega cm]$
ρ_i	Intracellular resistivity $[k\Omega cm]$
τ	Time variable to reach the steady state [ms]
m, n, h	Gating variables, probability for a membrane gating process

Contents

Chapter 1

Introduction

1.1 Motivation

Millions of patients are losing their vision all over the world due to retinal degenerative diseases. These diseases include Retinitis pigmentosa, age-related Macular Degeneration, or even accidents and injuries. This number is currently around 39 million worldwide [Shepherd et al.(2013)]. Losing sight is one of the most debilitating disorders since it severely influences the quality of life and diminishes it. Despite all physical restrictions, lack of this sense results in numerous psychological consequences such as insomnia, social isolation, or even suicidal thoughts.

Some of these injuries and diseases can be prevented or treated. Others such as Retinitis pigmentosa have no cure because they affect the neural network of the retina. Many worldwide researchers are targeting this group of diseases by using some approaches. For instance, stem cell transplants are one of the promising therapy for degenerated photoreceptors [Ramsaden et al.(2013); Chader et al.(2016)]. With considering the stem cells ability to differentiate into any cell, these cells can be used to reconstruct the damaged cells. However, there are many

challenges in this method that need to be overcome. Another approach is to replace damaged parts of the retina by engineered living tissues, microfabricated photoreceptor arrays, and an implantable electronic microsystem which are referred to as the visual prostheses. Visual prostheses receive image information from the out sight and deliver them to the natural visual pathway to provide a meaningful perception of the image which is done by passing failing parts of the visual pathway and releasing the information to the rest of the network. These implantable microsystems are designed and developed to either stimulate the nervous system or directly record neural activities with a high spatial resolution [Prochazka et al.(2001)]. The cochlear implants can be named as a successful example of these neural prostheses that has provided partial hearing to more than 120,000 persons worldwide at the end of the year 2008 [Zeng et al.(2008)].

The idea of electrically stimulating the human visual system was first appeared by Franklin [Isaacson et al.(2003)], Cavallo et al.(1777), and LeRoy in the 18th century [LeRoy et al.(1755)]. LeRoy produced visual sensations of light by passing an electrical charge through the eye of a blind man. In 1929, Foerster, a German neurosurgeon, observed a visual neural response to electrical stimulation when his patient saw a spot of light during the electrical stimulation of his visual cortex [Foerster et al.(1929)]. Since then, the approaches have moved from a distant dream to the near future reality. While the biological approaches are providing hope, stimulation of the visual system is the only useful option which has reached the clinical practice. Stimulation has provided appropriate solutions, or it has at least some functional vision for many patients all over the world [Barnes et al.(2016); da Cruz et al.(2016)]. Compared to other various stimulation sites such as the visual cortex [Lewis et al.(2016)], the optic nerve [Lane et al.(2016)], the lateral geniculate nucleus [Nguyen et al.(2016)], and the retina [da Cruz et al.(2016)], the electrical stimulation of the retinal neurons has several more advantages. For instance, the surgical risks associated with the implantation of the electrodes are considerably lower compared to other visual neurostimulators [Weiland et al.(2005)]. Retinal electrostimulation requires some microelectrodes to be implanted in the epiretinal [Duncan et al.(2017)],

subretinal [Stingl et al.(2015)], or in supra-choroidal space [Barriga-Rivera et al.(2017)] to activate the ganglion cells either directly or indirectly via the remaining pathway neurons. From previous studies and researches, it is demonstrated that the sufficiency and intensity of a stimulus are significantly effective but also controversial. Recent pieces of evidence have shown strong stimuli result in a reduction of neuron responses. Therefore, this study focused on different stimuli with different intensities, frequencies, and shapes for both intra and extracellular stimulation. A noise related approach is also investigated to simulate the condition of the experiment as analogous as possible.

1.2 Structure of thesis

In chapter 2, some necessary information about the visual pathway, retina anatomy and some basic explanation about neurons is given, In the next step some different modelling systems are briefly introduced. At the end of the chapter, some mathematical solving methods for differential equation will be introduced.

In chapter 3 all methods which have been used in simulation processes will be briefly explained. The Hodgkin-Huxley model, single and multi-compartment model will be discussed. Moreover, finally, the morphology of the diffuse bipolar DB4 which is used in this study will be given such as channel distributions.

In chapter 4 some intra and extra stimulation with different pulse shapes and frequencies in four regions of the cell is accomplished and compared. Finally, Gaussian white noise has been added to simulations to mimic the stochastic nature of biological signals and compare it with previous results.

In chapter 5, the results of the stimulations are summarised and discussed. additionally, the conclusion of this thesis are given.

Chapter 2

Background

2.1 Visual pathway

When the light enters cornea, it is projected onto the back of the eye. In that stage, the retina converts the light into the electrical signals. The signals are transferred through different retinal cells and two main layers of synaptic contacts. Then, the optic nerve that is formed by axons from retinal ganglion cells receives the electrical signals. The signals reach the visual cortex through the optic nerves. At the visual cortex, the brain processes the sensory data and responds appropriately. It is known that nearly half of all cortical neurons are devoted to the processing of the visual information [Lagrze et al.(2008)].

2.2 Retina anatomy

The vertebrate retina is consist of five main neural cells and nine different layers. It is approximately 0.5 mm thick and has a diameter of approximately 30-40 mm [Polak et al(1941); Lagrez et al.(2008)].

Retinal neural cells:

- First neuron: photoreceptors
- Second neuron: bipolar cells
- Third and fourth neurons: horizontal cells and Amacrine cells
- Fifth neuron: retinal ganglion cells

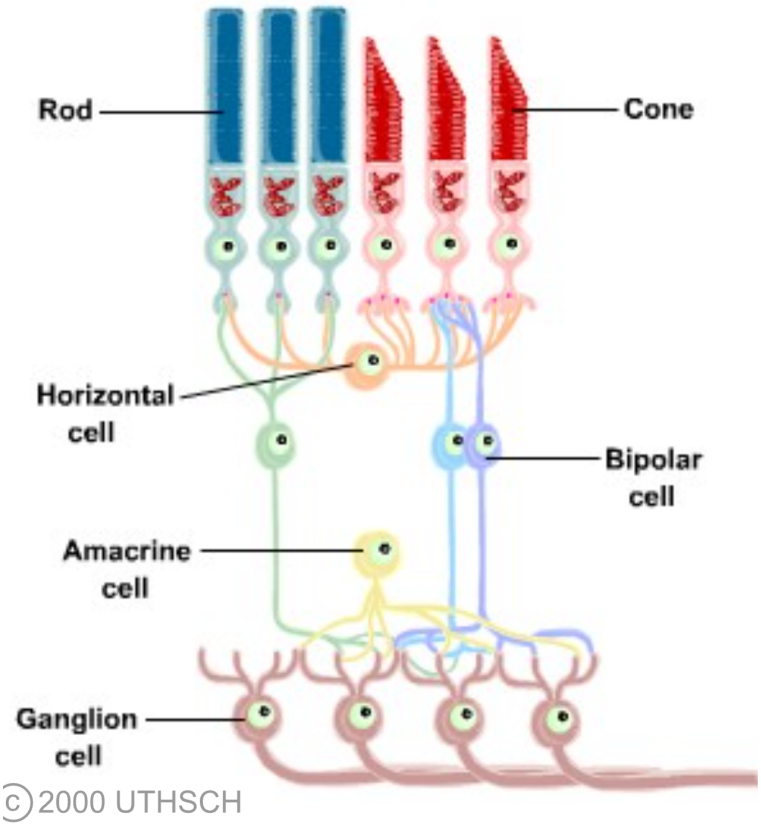

Figure 2.1: Retinal neurons (taken from eye and retina, McGovern Medical School, University of Texas)

Retinal layers: [Blakeslee et al.(2015)]

- **Inner limiting membrane:** This layer is the boundary between the vitreous humour in the posterior chamber and the retina.
- **Ganglion cell layer:** Consists of ganglion cell bodies and axons.
- **Inner Plexiform Layer(IPL):** Contains synapses made between bipolar, amacrine and ganglion cells.
- **Inner nuclear layer:** Contains bipolar, horizontal and amacrine cell bodies.
- **Outer Plexiform Layer(OPL):** Contains bipolar cell, horizontal cell and receptor synapses.
- **Outer nuclear layer:** Contains the nuclei of photoreceptors.
- **Outer limiting membrane:** A membrane which coincides with the base of inner segments of a photoreceptor.
- **Photoreceptor layer:** Consists of the inner and outer segments of rod and cone photoreceptors.
- **Pigment epithelium:** Consists of the darkly pigmented cells which absorb light not captured by photoreceptors to reduce scattering.

2.2.1 Photoreceptors

Photoreceptors (PRs) in the human are classified into two groups of cells, the rods (Low-Light) and the cones (High-Light). The human retina contains about 130 million rods [Osterberg et al.(1935)] which are more sensitive than cones since they are responsible for tiny amounts of light or so-called scotopic vision. Rods contain the photopigment rhodopsin which is composed

of a protein part, opsin and retinal. This protein part is an aldehyde of the vitamin A molecule. Cones are about 6 million in the human retina, and they are mostly found in the centre of the fovea [Osterberg et al.(1935)]. Cones are responsible for photopic vision, vision in the intense light. They are responsible for the perception of shapes and colours as well. The opsin structure of photopigment of cones differs from rods. Therefore, three different types of cones absorb light of different wavelengths depending on the different types of cone opsin. One type responds to light in the blue part of the spectrum (maximum wavelength 420 nm), another response to the green part of the spectrum (maximum wavelength 530 nm), and the third type responds to the red part of the spectrum (maximum wavelength 560 nm).

2.2.2 Bipolar cells

Bipolar cells (BCs) transfer signals from rod and con PRs and ganglion cells. This transformation can be either directly or indirectly through the amacrine cells. They also accept synapses from horizontal cells. The rod BCs only make connections to rods [Boycot et al.(1969)]. There are approximately about 912 kinds of cone BC while there is only one rod BC in the mammalian species that have been studied thoroughly [Sheasby et al.(1999)]. It is known that BCs communicate via graded potentials rather than action potentials.

In the absence of light, the PRs release a neurotransmitter named glutamate. This neurotransmitter inhibits (hyperpolarise) the ON BCs and excites (depolarise) the OFF BCs. If light enters, it strikes the PRs and results in their inhibition. Then the opsin is activated and causes all trans-retinal activation which will produce the required energy to stimulate G-protein and activates phosphodiesterase that breaks cGMP into 5'-GMP. When there is less light, cGMP in PRs are high. Therefore, this will keep some Na channels open; the activated phosphodiesterase reduces the amount of cGMP, and the open Na channels. As a result, hyperpolarising the PRs is terminated; hence, less glutamate is released which will cause the ON BCs to lose their inhibition, and become depolarised while the OFF BCs lose their excitation and become

hyperpolarised [Purves et al.(2008)].

2.2.3 Retinal Ganglion cells

Finally, the ganglion cells (GCs) receive information from PRs and transform it into trains of action potentials (APs) through their axons. They receive the signals through either the BCs or through the retina amacrine cells. GCs are divided into several subclasses of mostly parasol and midget cells [Soto et al.(2011)] regarding their sizes, dendritic branching level, and their measured electrophysiology. There are ON and OFF GCs which are connected with either ON or OFF BCs. The ON GCs are excited when the light hits the centre of their receptive fields and inhibited when the light hits the periphery of their receptive field. Parasol cells compose about 80% of all GCs. They are colour specific and have small receptive fields, therefore, are involved with the form and colour. On the other hand, Midget cells have larger receptive fields, respond optimally to the large objects, and can follow rapid changes in the stimulus [Kandel et al.(2000)].

2.2.4 Interneurons of the retina

There are two more cell types in the retina that are responsible for signal processing. Amacrine and horizontal cells (ACs and HCs). ACs are a significant fraction of retinal neurons, and they are divided into about 30 types [Kolb et al.(1981)] based on their dendritic sizes and their stratification stratum within the IPL. ACs are intercalated between the axons of BCs and the dendrite of GCs. They are responsible for interactions between ON and OFF synaptic centres by releasing different neurotransmitters [Masland et al.(2012)]. Therefore, they are crucial for the increase of contrast and motion detection. HCs are smaller in number compared to the other retinal neurons. They are known to control contrast levels between the dark and the light regions.

2.2.5 What is a neuron?

Neurons communicate with electrical signals which are generated in response to chemicals and other inputs through their dendrite and axons. Some of the most common types of neurons are shown in Figure 2.2. The dendrite is the receiver side of the neuron while the axon carries the neural output to the other cells. The expanded form of dendrite allows a neuron to achieve the information from many other neurons. This transmission of the electrical signals from one neuron to another happens through synaptic connections. Figure 2.2 does not show the axons and dendrites of these neurons to the full extent. An axon can travel a considerable distance inside the brain or even in some cases can travel inside the entire body.

In addition to all the morphological features that a neuron has, it has many physiological specialisations such as ion channels, the pore-forming membrane proteins. There are various types of ion channels which differ in their shapes and operations. These ion channels allow specific ions such as sodium (Na^+), potassium (K^+) , calcium (Ca^{2+}) and chloride (Cl^-) to pass through the cell. Their functions include establishing a resting membrane potential, shaping action potentials, and other electrical signals by gating the flow of ions across the cell membrane, controlling the flow of ions across secretory and epithelial cells, and regulating cell volume. Ion channels are present in the membranes of all excitable cells such as neurons. Each neuron has a resting potential which is the difference in electrical potential between the inside and the surrounding extracellular medium. This potential is about -70 mV. Ion pumps inside the cell membrane maintain concentration gradients that support the resting potential. For instance, while the concentration of (K^+)is remarkably higher inside a neuron, (Na^+) is significantly concentrated outside of the cell. There are two gradients, potential and concentration gradient, which cause the ions to flow through the cell membrane. When positive ions flow into the cell, the membrane potential becomes less negative or even positive which is called depolarisation. With positive ions flowing out of the cell, the membrane potential becomes more negative which is called hyperpolarisation.

When a neuron is depolarised, and its membrane potential goes above a threshold level, which is much linked to the type of the cell, an Action Potential (AP) is initiated. For a few milliseconds right after when an AP has been fired, it may be impossible for another spike to occur which called the absolute refractory time. The relative refractory period is referred to a longer interval during which it is complicated but not impossible for another AP to occur. APs are the only forms of the membrane fluctuations that can propagate over the vast distances, and the subthreshold potential fluctuations are generally attenuated after 1 mm or less. On the other hand, APs are regenerated along the axon and can travel without attenuation.

At the end of axons, synapses are located. After an AP reaches the synapse terminals, some ion channels open and produce an influx of Ca^{2+}. Releasing of Ca^{2+} leads to the release of neurotransmitters which binds to the postsynaptic side and causes ion-conducting channels to open. Synapses have either an excitatory, depolarising, or an inhibitory, hyperpolarising, effect on the postsynaptic neuron and this depends on their nature of the ion flow.

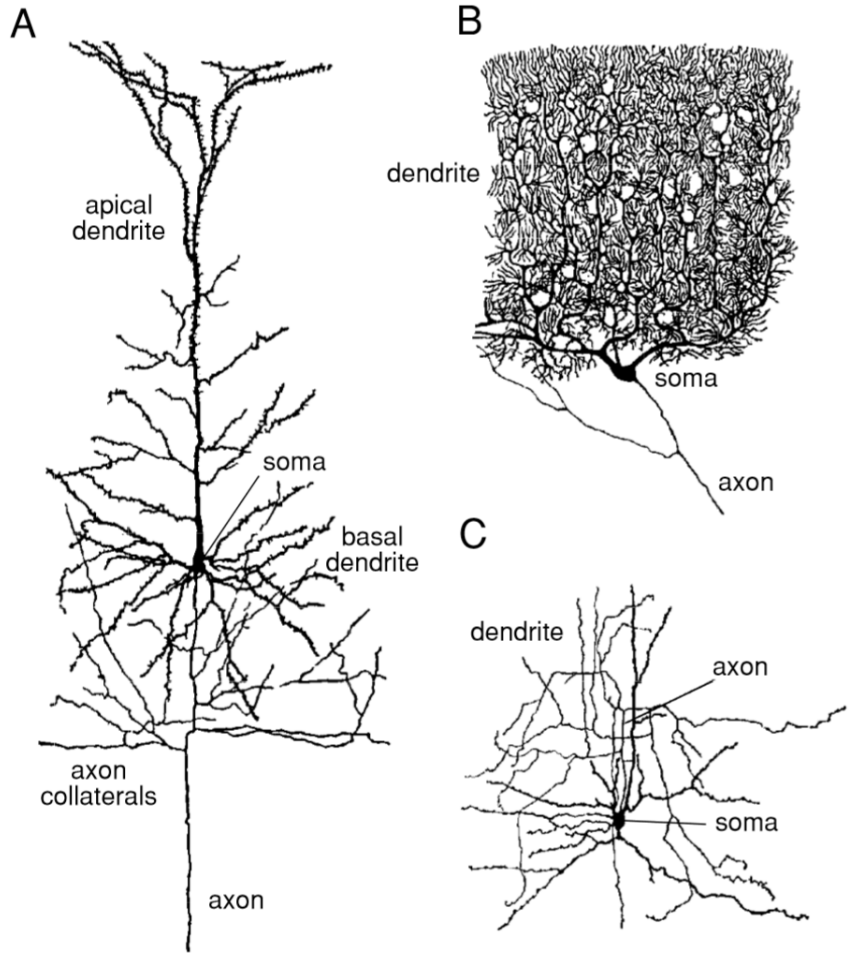

Figure 2.2: Digram of three neuron (A) A cortical pyramidal cell. (B) A Purkinje cell of the cerebellum. (C) A stellate cell of the cerebral cortex. (Drawing from Cajal,(1911); figure from Dowling,(1992))

2.3 Computational neuroscience

In this section, some mathematical and solving models which are commonly used for modelling in computational neuroscience will be briefly explained.

2.3.1 Mathematical methods

A mathematical model should be created to understand the behaviour of a natural system such as neurons. A mathematical model includes the dynamic of the system, statistical models, and differential equations. However, a model is suitable when the development of the model on the theoretical side agrees with the result of the experiment.
Mathematical and statistical models have played essential roles in neuroscience, especially by describing the electrical activity of neurons recorded individually or collectively across the large networks. However, new challenges are emerging as this field is growing and moving forward rapidly.
Many different mathematical models for neurons have been proposed so far. These models can be found based on either electrical membrane voltage models, pharmacological models, or natural models. A few different examples of the first group is listed below to help to focus more on the main point of this study.

- **Integrate-and-fire:**

  The integrate-and-fire model has a long and distinguished history going back to Lapicque (1907, 1926), which was before anything specific was known about the biophysics of excitable membranes. Some people have analysed more recent versions of this model. The model assumes that a voltage threshold governs spike initiation. When the somatic membrane potential exceeds that threshold, a spike is fired, and the membrane potential

is reset back to V-rest. In its simplest form, the membrane potential is assumed to literally integrate the input current:

$$I(t) = C_m \times dV/dt \tag{2.1}$$

Where C_m is the membrane capacitance, V is the membrane potential, and I is the input current [Abbott et al.(1999)].

- **Leaky integrate-and-fire:**

  This is a much more palatable version which assumes that the neuron is a single passive compartment. Then the membrane potential charges and discharges exponentially in response to the injected current:

$$C_m \times dV/dt + g_L \times V_L(t) = 0 \tag{2.2}$$

  Where g_L is the leak conductance, and V is the membrane potential with respect to the rest. The leaky integrate-and- fire model has been applied to model the firing behaviour of many cells such as neurons in the Limulus eye and cortical cells [Koch et al.(1999)].

- **Hodgkin-Huxley model:**

  The Hodgkin-Huxley model (HH model) is established by Alan Lloyd Hodgkin and Andrew Fielding Huxley in 1952 [Hodgkin and Huxley et al.(1952a)]. This model is based on the concept of membrane ion channels and relies on data from the squid giant axon. Hodgkin and Huxley were awarded the 1963 Nobel Prize in Physiology or Medicine for this model. The model includes multiple voltage-dependent currents which are given by the Ohm's Law.

$$I = C_m \times V/dt + g_K(V - V_K) + g_l(V - V_L) + g_{Na}(V - V_{Na}) \tag{2.3}$$

where I is the total membrane current per unit area, C_m is the membrane capacitance per unit area, g_K and g_{Na} are the potassium and sodium conductance per unit area, respectively, V_K and V_{Na} are the potassium and sodium potentials, respectively, and g_L and V_L are the leak conductance per unit area and leak potential, respectively. The time dependent elements of this equation are V, g_{Na}, and g_K, where the last two conductances depend explicitly on the voltage as well.

2.3.2 Solving methods

After choosing the suitable model, a series of differential equations (DEs) are obtained. To get the appropriate results, DEs should be solved either analytically or numerically. However, it is suggested to solve these equations numerically since an analytical solution for such sophisticated equations is far-fetched. There are different solving methods to find numerical approximations to the exact solution of a DE [Gear et al(1971); Stoer et al.(1980)].

- **Forward Euler method (explicit):**

$$y_{n+1} = y_n + f(y_n, t_n) \times h \tag{2.4}$$

The forward Euler method is based on a truncated Taylor series expansion. The advantage of the Forward Euler method is that it has a simple implementation. It is evident that an error is induced at every step due to the truncation of the Taylor series, this is referred to as the local truncation error (LTE) of the method. For the forward Euler method, the LTE is $O(h^2)$. Hence, the method is referred to as a first-order technique. In general, a method with $O(h^k + 1)$ LTE is said to be of kth order. Higher order techniques provide lower LTE for the same step size. However, in the case of instabilities, the method is not valid anymore. Implicit methods can be used to replace explicit ones in cases where

the stability requirements of the latter impose stringent conditions on the time step size.

- **Backward Euler method (implicit):**

  Implicit methods such as BE are more expensive to be implemented for non-linear problems since y_{n+1} is given only concerning an implicit equation. The implicit analogue of the explicit FE method is the backward Euler (BE) method. This is based on the following Taylor series expansion.

$$y_{n+1} = y_n + f(y_{n+1}, t_{n+1}) \times h \tag{2.5}$$

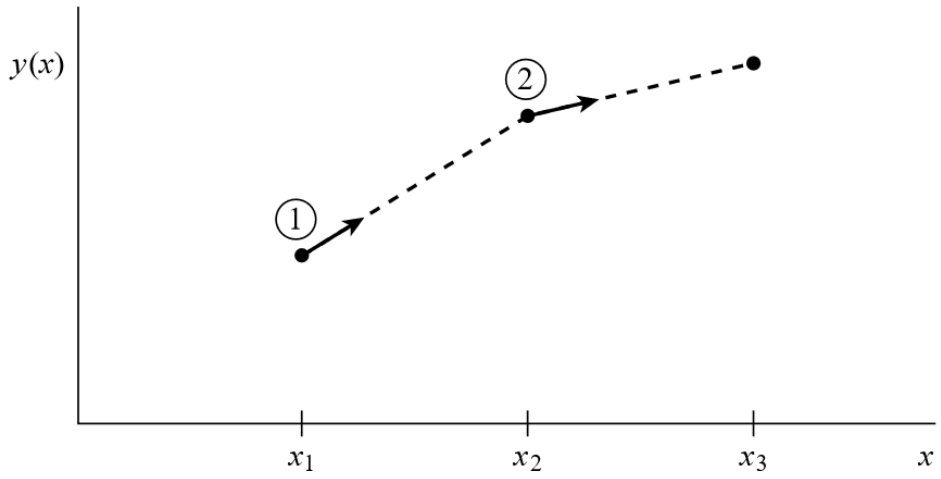

Figure 2.3: Euler's method. In this simplest (and least accurate) method for integrating an ODE, the derivative at the starting point of each interval is extrapolated to find the next function value. The method has first-order accuracy.

- **Runge-Kutta:**

  Runge-Kutta or midpoint method is a numerical method to solve a differential equation. This method uses trial steps at the midpoint of intervals to eliminate lower-order errors. It is reasonably straightforward, robust, and is an excellent general candidate for the numerical solution of differential equations when combined with an intelligent adaptive

step-size routine. Runge-Kutta was developed around 1900 by the German mathematicians C. Runge and M. W. Kutta. The fourth method of Runge-Kutta which is the most accurate one is written as:

$$
\begin{aligned}
&y_{n+1} = y_n + \frac{1}{6} \times (k_1 + 2k_2 + 2k_3 + k4) \\
&t_{n+1} = t_n + h \\
&For\ n = 0, 1, 2, ... \\
&k_1 = hf(t_n, y_n), \\
&k_2 = hf(t_n + \frac{h}{2}, y_n + \frac{k_1}{2}), \\
&k_3 = hf(t_n + \frac{h}{2}, y_n + \frac{k_2}{2}), \\
&k_4 = hf(t_n + h, y_n + k_3).
\end{aligned}
\tag{2.6}
$$

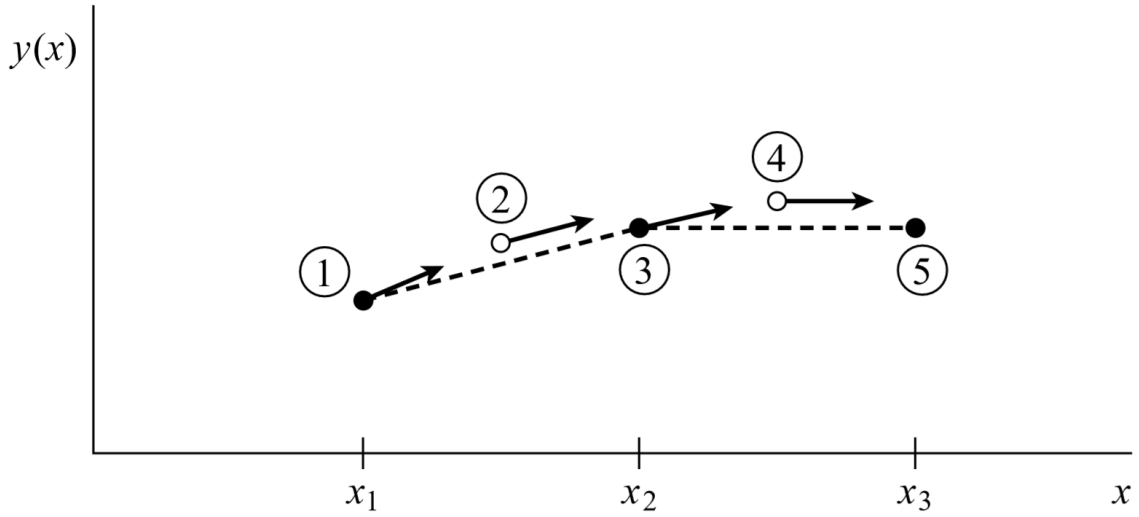

Figure 2.4: Runge-Kutta method. Second-order accuracy is obtained by using the initial derivative at each step to find a point halfway across the interval, then using the midpoint derivative across the full width of the interval. In the figure, filled dots represent final function values while open dots represent function values that are discarded once their derivatives have been calculated and used.

2.4 Single soma example

Here a simple example has been provided to help with a better understanding of the previously given information. The example shows the initiation of an AP after running an intracellular stimulation, 10 pA, of a single soma with 10 micrometre of diameter. The simulation is done through Python (Version 2.7), and the Runge-Kutta method is used as the solver. Current fluctuations across the membrane are considered as a noisy component that is added to the stimulus. The aim of this section is to give a concise overview of all previous sections and to show how an AP has occurred. Further complementary information is given in the next chapters.

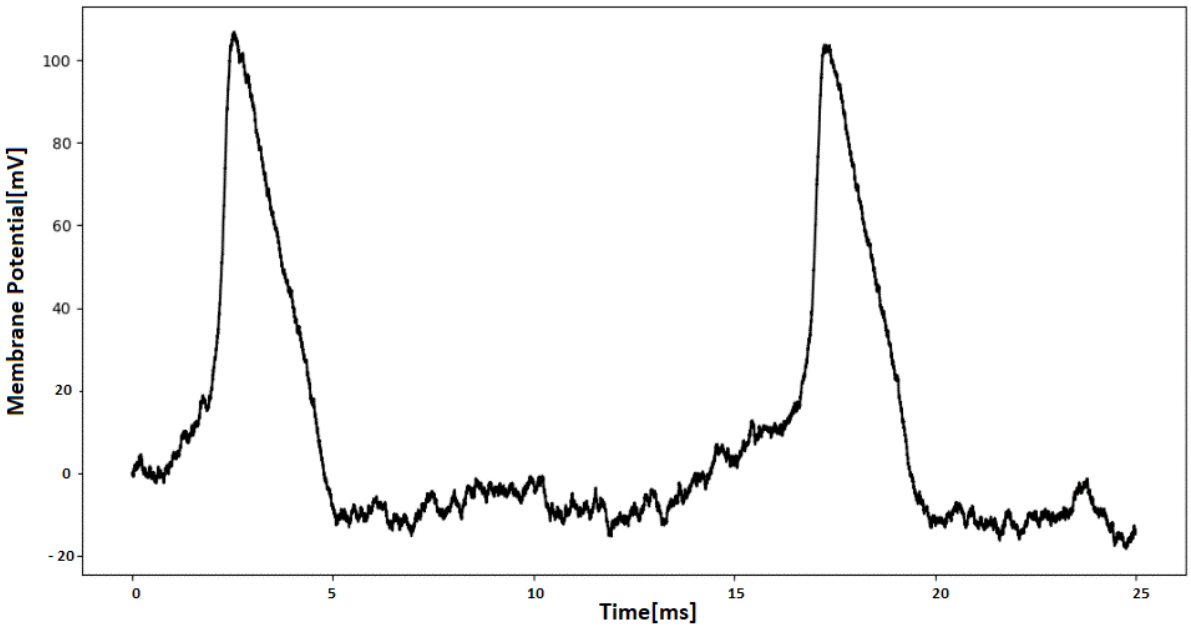

Figure 2.5: Intracellilar stimulation of a single soma with current injection of 10 pA

Chapter 3

Methods and Materials

In this section, all applied methods and the morphometry of the used cell (DB4) are briefly explained. Additionally, a simple multi-compartment model example is done to give an idea on how to make the axial matrix from an SWC file. Another example has been done to explain the application of the Hodgkin-Huxley model for a single soma. In the end, the morphometry of the DB4 is shortly explained.

3.1 Compartmental model

A physiologic system such as a neuron is often described by decomposition into a number of interacting subsystems, called compartments. Compartments should not be understood as a physical volume, but rather as a mass of well-mixed, homogeneous material that behaves uniformly. Each compartment may exchange material with other compartments. This model is the most common model used in computational neuroscience. Compartmental model is defined either for a single neuron element, single-compartment or for multi-elements such as a whole neuron, multi-compartment, which is represented in this study.

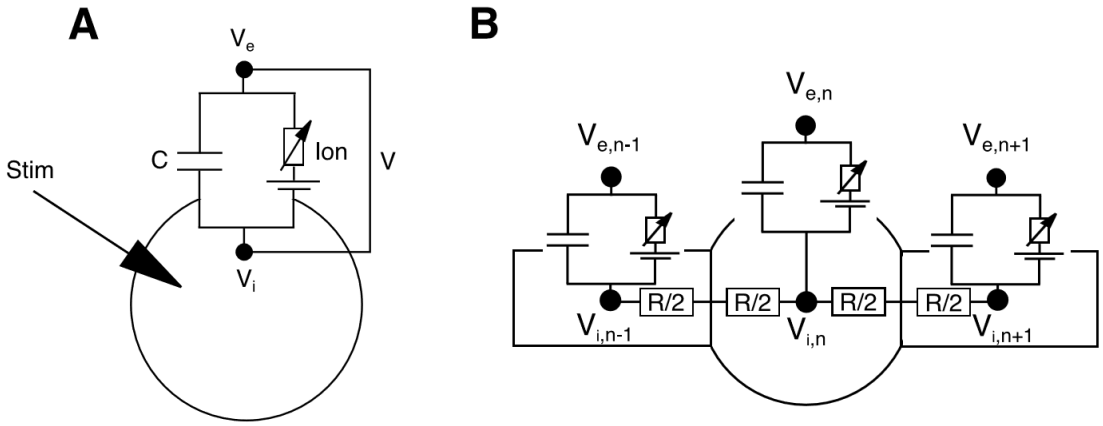

Figure 3.1: Single and multi-compartment models

3.1.1 Passive model

Considering a single compartment model as shown in Figure 3.1 A, a passive membrane is defined by a simple model which consists no non-linearity of cell behaviour. In a passive model, the term of ion current includes only the leakage current as:

$$I_{ion} = I_G = G_L \times (V - E_L) \tag{3.1}$$

The G_L represents the leakage channels which has a relatively low conductance in mS and does not change, made up by chloride and other ions. In the passive membrane model leakage channels are mainly responsible for the resting membrane potential. Therefore, the E_L, leakage potential is almost equal to the rest potential. The V indicates the membrane which is the difference between intra- and extracellular potentials ($V = V_i - V_e$). All potentials are represented in mV. By applying the Kirchhoffs first law:

$$I_{ion} + I_{stim} + I_{C_m} = 0 \rightarrow \frac{dV}{dt} \times C_m + I_{ion} + I_{stim} = 0 \tag{3.2}$$

In equation, I_{stim} represents the injected current, C_m represents the membrane capacitance in μF. All currents have the unit $\mu A/cm^2$.

3.1.2 Active model

An active model refers to a model of the cell which includes the potassium and the sodium currents as well as the leakage. The active membrane has been accomplished by the Hodgkin-Huxley model and implemented in this study.

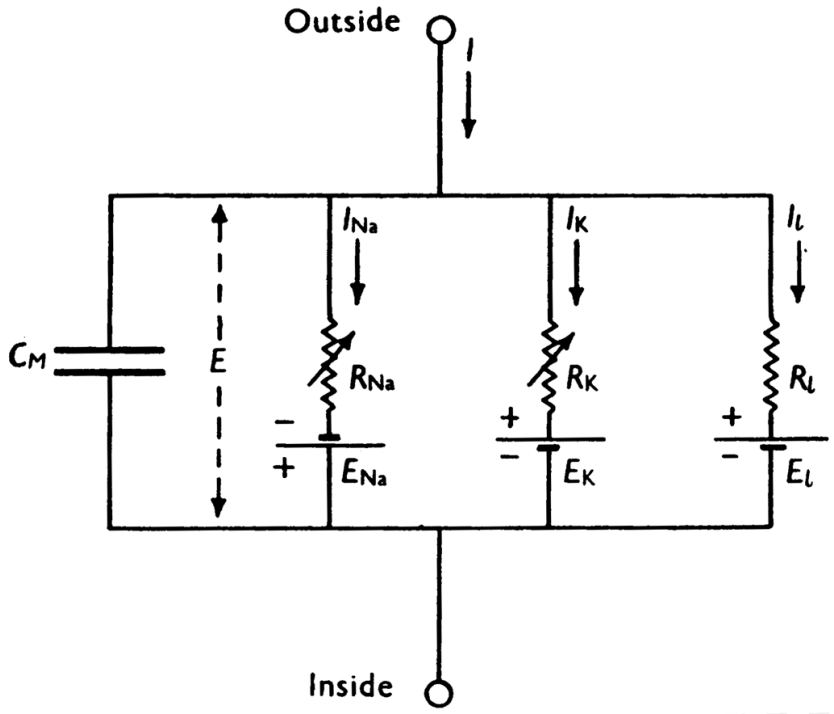

Figure 3.2: Electrical circuit representing membrane(taken from Hodgkin and Huxley et al.(1952b))

The Hodgkin-Huxley (HH) model for the generation of the nerve action potential of an active model is one of the most successful mathematical models of a complicated biological process that has ever been formulated. The basic concepts expressed in the model have proved a valid approach to the study of bio-electrical activity through to the neurons within the nervous system [Hodgkin and Huxley et al.(1952b)]. The HH model will be explained in more details in section 2.2. The I_{ion} in an active model contains all presented ion channels such as sodium and

potassium channels. For more than one compartment the axial current should be considered. The axial current is a current which flows through the model. The current equation needs to be extended by adding the axial current term as shown in Equation 3.3 for the nth compartment.

$$\begin{aligned} &I_{ion} + I_{st} + I_C + I_{ax} = 0 \rightarrow \frac{dV}{dt} \times C_m + I_{ion} + I_{stim} + I_{ax} = 0 \\ &I_{ax}(n) = \frac{V_n - V_{n-1}}{\frac{R_n}{2} + \frac{R_{n-1}}{2}} + \frac{V_n - V_{n+1}}{\frac{R_n}{2} + \frac{R_{n+1}}{2}} + ... \end{aligned} \tag{3.3}$$

Whereas V_{n-1} and V_{n+1} represent the adjacent neighbours to the nth compartment and $R_n/2$ refers to the resistance from the midpoint to the end of a compartment with a unit of $k\Omega/cm^2$. For a cylindrical compartment R_n is written as:

$$R_n = \frac{\rho_i \times l}{A} \rightarrow R_n/2 = \frac{\rho_i \times l}{2r2n\pi} \tag{3.4}$$

Where A representing the cross-section surface in cm^2, ρ_i the specific intracellular resistivity in $k\Omega cm$, l_n the compartment length and r_n the radius of the compartment. To calculate I_{ax} for a multi-compartment model, first, the adjacency matrix and second the axial matrix M were calculated, finally the axial matrix was multiplied with the voltage vector V. The adjacency matrix is a square matrix used to represent the compartment graph. The elements of this matrix indicate whether the compartments are adjacent or not.

$$I_{ax} = M \times V \tag{3.5}$$

The adjacency matrix is extracted from the SWC file of the neuron morphology and contains 0 and 1 which refer to either the compartments are not connected or connected, respectively.

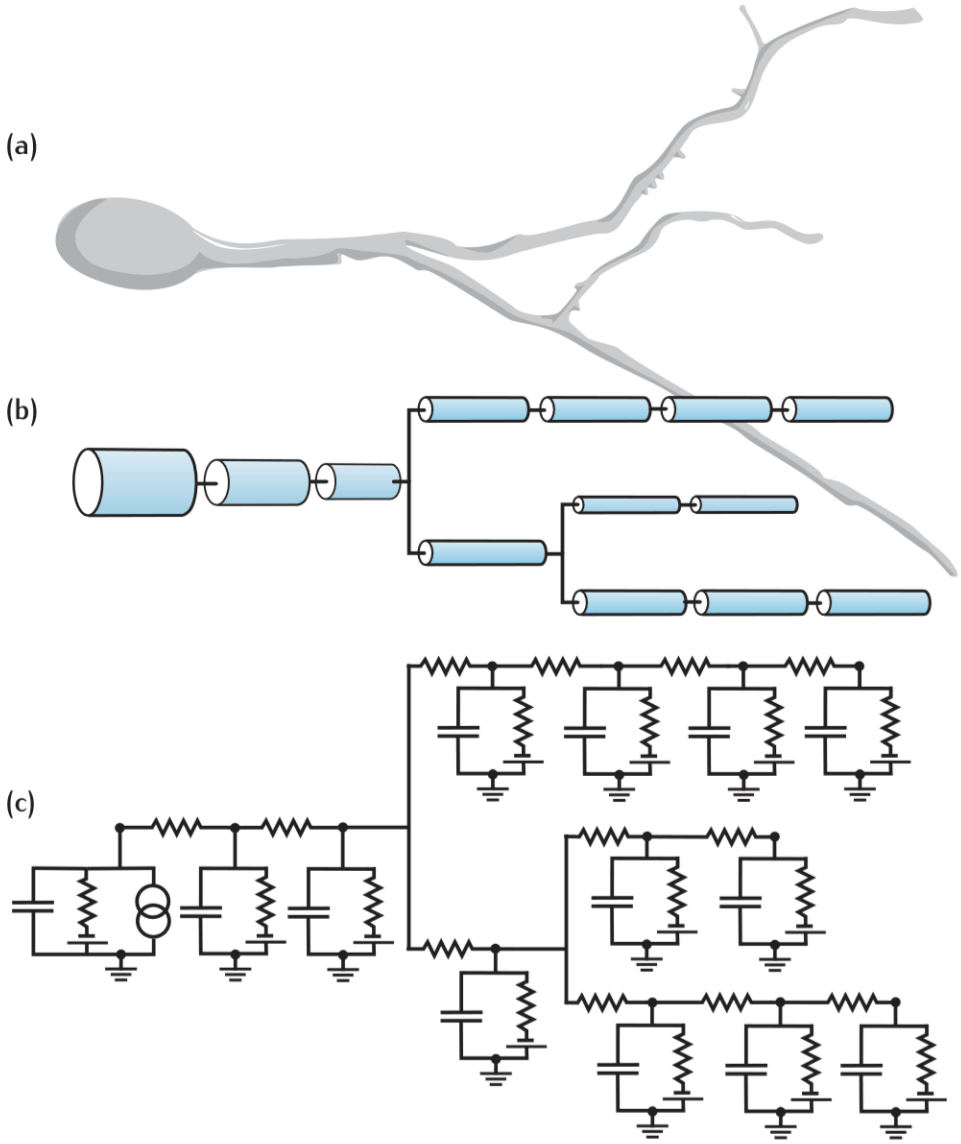

Figure 3.3: A diagram of the development of a multi-compartmental model. (a) The cell morphology is represented by (b) a set of connected cylinders. An electrical circuit consisting of (c) interconnected RC circuits is then built from the geometrical properties of the cylinders, together with the membrane properties of the cell [Sterratt et al.(2011)].

3.1.3 Obtaining axial matrix M

Extraction of M is a crucial step for simulation aims. Therefore, for a profound understanding of the matter, a simple example is provided. However, there are many methods to obtain an axial Matrix which is completely optional. The following method is a simple way, suitable for an irregular numbering system and has been chosen for the simulations in this report.

Example model:

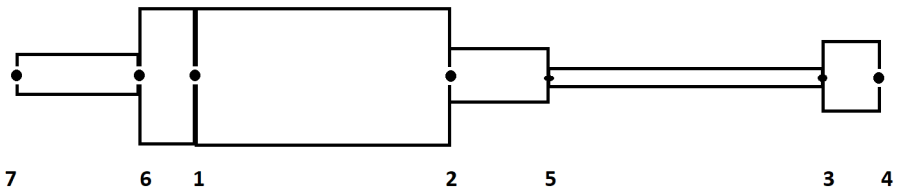

Figure 3.4: A simplified 6 compartments Example]

The SWC file is:

Table 3.1: The SWC file information

ID	TYPE	X	Y	Z	RADIUS	PARENT
1	1	0	0	0	5	-1
2	1	0	0	-5	5	1
3	3	0	0	-11	2	5
4	4	0	0	-13	3	3
5	1	0	0	-7	4	2
6	1	0	0	1	5	1
7	6	0	0	4	2	6

SWC is a format to store a cell morphology. The content of an SWC file is shown in Table 3.1. The ID stands for an index of each compartment and depends on how the compartments were

ordered and numbered. For instance either by choosing an arbitrary branch and numbering its compartment and repeating the process until all compartments are numbered or by starting from the soma and going through all compartments. The second procedure has been chosen for this study. The TYPE represents the compartment origin within the cell such as soma, dendrite, axon etc. X, Y and Z are the coordinates of the endpoints of each compartment. Radius is the compartment radius, and PARENT stands for the start coordinate. All coordinates and radius units are in μm and should be converted to cm before using them in the main equations. Since the soma is always the start point, therefore its parent is shown by -1. The following steps can be done either with MATLAB or PYTHON. In this study, all simulations were performed using the Python (Version 2.7)

- **Calculation of the length of the compartments:**

  This step is done by a very simple calculating of the distance between two continuous compartments which indicate the start and the end coordinates.

- **Midpoints:**

  In this step, midpoints are calculated, and this is an essential step for applying an external stimulation to compute the distance between all compartments and the electrode position. More relevant information is provided in the Result chapter.

- **Elimination of the first compartment:**

  In this step, the first element of all vectors, obtained from SWC file (ID, PARENT, Midpoints, Length and RADIUS), will be eliminated but before doing it, following steps need to be done. This step is crucial to order all compartment whereas all begin with soma which is set to 1.

  1. First, the ID and PARENT should be subtracted by one (to remove -1 from the data and convert it to a 0).
  2. Second, the PARENTs which are equal to 0 should be added by one

3. Finally, the first elements of all vectors need to be eliminated.

After applying this step the new IDs, PARENTs and RADIUSes are:

Table 3.2: The Modified SWC file

ID	PARENT	RADIUS
1	1	5
2	4	2
3	2	2
4	1	5
5	1	2
6	5	2

- **Adjacency matrix:**

  In this step, a square Matrix, which has the same dimension as the number of compartments, should be created. Therefore the dimension in this particular example is 6×6. This should be taken into care that in all next steps, the new IDs and PARENTs are used. Firstly, the relevant graph from the new IDs and PARENTs is created. In this investigation, it was done by NETWORKX module of python (version 2.7). Secondly, since no compartment is related to itself, therefore all main diagonal elements need to be zero. The relevant graph and adjacency matrix for this example are shown in the Figure 3.5

- **Calculating of every compartment resistance R_i:**

  Since all lengths and areas were calculated in previous steps, this step is done by just applying Equation 3.4 for every compartment.

- **Axial matrix:**

  According to I_{ax} , term $1/(Ri/2 + Rj/2)$, with i and j representing current row and

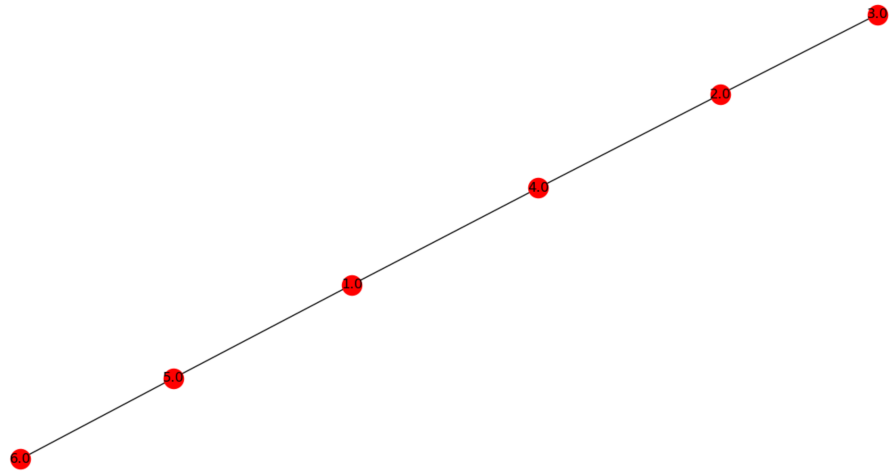

$$\begin{bmatrix} 0 & 0 & 0 & 1 & 1 & 0 \\ 0 & 0 & 1 & 1 & 0 & 0 \\ 0 & 1 & 0 & 0 & 0 & 0 \\ 1 & 1 & 0 & 0 & 0 & 0 \\ 1 & 0 & 0 & 0 & 0 & 1 \\ 0 & 0 & 0 & 0 & 1 & 0 \end{bmatrix}$$

Figure 3.5: left represents corresponding graph and right represents adjacency matrix of 6 compartments example

column, is multiplied to the adjacency matrix. Then, the main diagonal elements should be the sum of all other elements in the same row. Since all currents are computed as current densities with units of $\mu A/cm^2$, the unit of the axial matrix needs to be $k\Omega/cm^2$. Thus all elements need to be divided to the relevant compartment surface.

3.2 Hodgkin-Huxley model

It is helpful to discuss the Hodgkin-Huxley model in more detail to have a better understanding of an active model which has been chosen in this study. In this section, all necessary equations for a reasonable simulation are described. More information in details can be found in a series of articles [Hodgkin and Huxley et al.(1952 a,b)]. The method used in the experimental work for the original study was based on the voltage clamp method. The voltage clamp is an experimental method used in electrophysiology to measure the ion current through the membrane while holding the membrane voltage at a set level. Transmembrane voltage is recorded through a voltage electrode, relative to ground, and a current electrode passes current

into the cell. The concept of the voltage clamp is attributed to Kenneth Cole and George Marmont in 1947. The total ionic current density in the Hodgkin-Huxley model is calculated by:

$$I_{ion} = G_{Na} \times (V - E_{Na}) + G_K \times (V - E_K) + G_L \times (V - E_L) \tag{3.6}$$

where I_{ion} denotes ionic current density. All voltages have computed from the Nernst equation:

$$E_X = \frac{R \times T}{2F} \times ln\frac{(X)_e}{(X)_i} \tag{3.7}$$

with R representing the gas constant ($8.3144621 J/molK$), T being the temperature in Kelvin and F the Faraday constant ($96485.3365 C/mol$). $(X)_i$ and $(X)_e$ denote the ion concentrations at the inside and outside of the cell, respectively. An essential factor should be taken into account that the original temperature at which the experiments have been done is at 6 °C, therefore, for any other temperature a temperature coefficient should be calculated which is more explained at the end of this chapter.

3.2.1 Ionic currents of the original HH model

- **Potassium current**

$$\begin{aligned} P_K = n^4 \ with \ 0 \leq n \leq 1 \\ G_K = g_K \times n^4 \end{aligned} \tag{3.8}$$

P_k represents the probability of gating particle in the open state. With α_n and β_n denoting changing state from close to open and from open to close respectively. And it can be modelled as:

$$\begin{aligned} \frac{dn}{dt} &= \alpha_n(V)(1-n) - \beta_n(V) \times n \\ G_K &= g_K \times n^4 \end{aligned} \tag{3.9}$$

α and β have been determined by Hodgkin and Huxley to fit the experiments. When the membrane voltage is fixed, the state variable will reach a steady state value and the time constant τ_x explains how long it takes to reach this steady state.

$$\begin{aligned} n_\infty &= \frac{\alpha_n(V)}{\alpha_n(V) + \beta_n(V)} \\ \tau_n &= \frac{1}{\alpha_n(V) + \beta_n(V)} \end{aligned} \tag{3.10}$$

- **Sodium current**

$$\begin{aligned} P_{Na} &= m^3 \times h \; with \; 0 \leq m, h \leq 1 \\ G_{Na} &= g_{Na} \times m^3 \times h \end{aligned} \tag{3.11}$$

With m and h being the probabilities for the open-close state of the activating and inactivating gates, respectively. The change of a state and the final conductance can be modelled as:

$$\begin{aligned} \frac{dm}{dt} &= \alpha_m(V) \times (1-m) - \beta_m(V) \\ \frac{dh}{dt} &= \alpha_h(V) \times (1-h) - \beta_h(V) \end{aligned} \tag{3.12}$$

Again the α and β have been determined by Hodgkin-Huxley to fit the experiments. The time constant and the steady state, with variable x which can be m or h, is written as:

$$x_\infty = \frac{\alpha_x(V)}{\alpha_x(V) + \beta_x(V)}$$
$$\tau_x = \frac{1}{\alpha_x(V) + \beta_x(V)} \tag{3.13}$$

- **Leakage current**

  Finally, the leakage conductance is equal to its value.

$$I_L = g_L \times (V - E_L) \; with \; E_L = -71.8mV \tag{3.14}$$

All equations have been solved through backward Euler solver which was explained in more detail in the background chapter, solving method section. For better understanding, in figures below an example of a simulation of a single soma is shown. The soma is stimulated with a rectangular current amplitude of 10 $\mu A/cm^2$ for 5 mS.

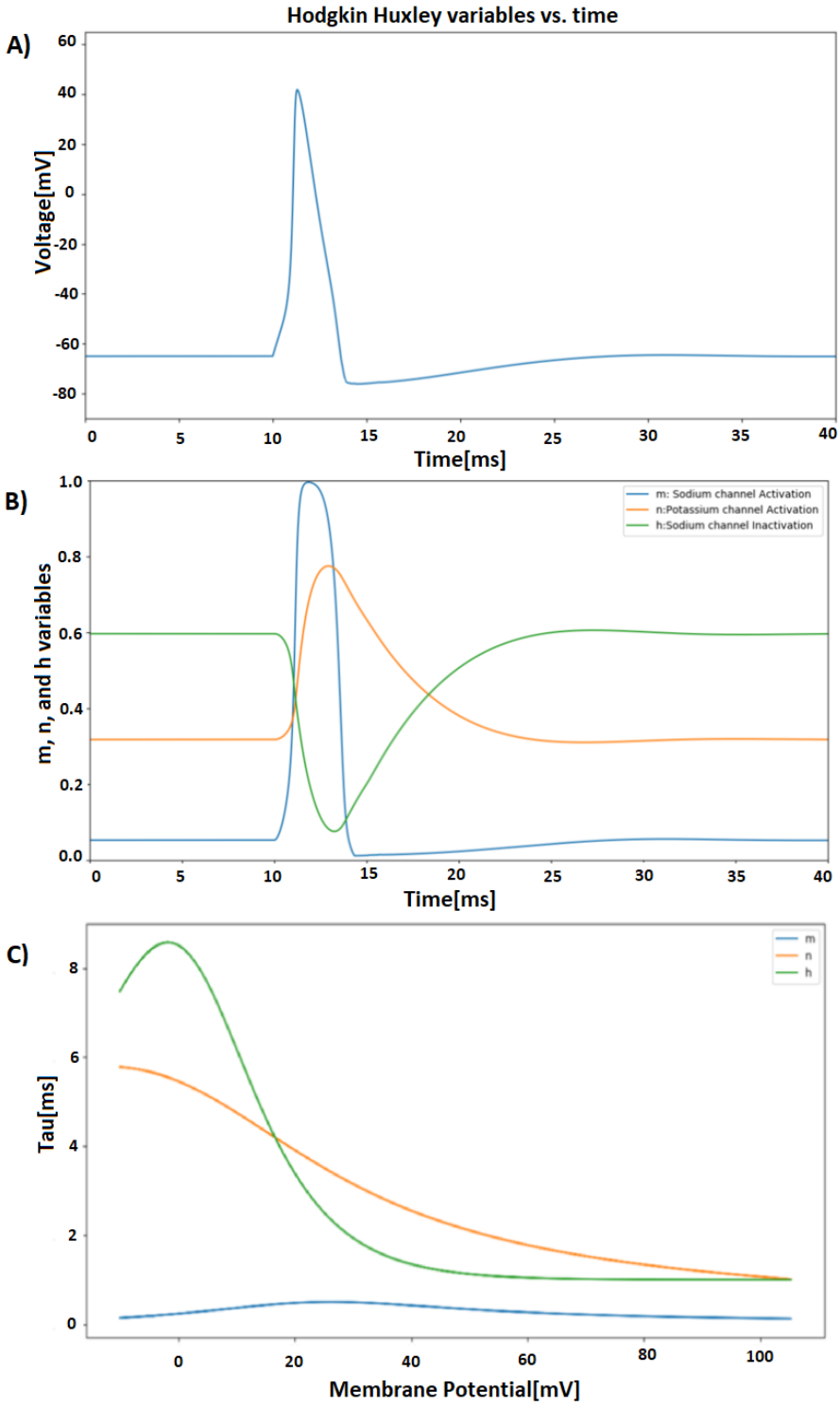

Figure 3.6: Single soma stimulation A)Membrane voltage curve B,C)sodium and potassium channel dynamics

3.3 Material

3.3.1 Diffuse Bipolar DB4 cell

For simulating purposes a diffuse bipolar DB4 of macaque has been used in this study and the cell morphology is obtained from [Puthussery et al.(2013)]. In Figure 3.8 in left, a 3-D model of the cell is shown. DB4 is an ON (cone) diffuse bipolar cell made reciprocal synapses with a kind of ON-OFF lateral amacrine cell, and the type is first outlined by Polyak [Polyak et al.(1941)]. A series of different bipolar cells has been shown in figure Table 3.3. The dendrites of all bipolar types stratify at the same level in the OPL, but the axons terminate type dependently in different strata ($1 \sim 5$) of the IPL. An important segment is the Axon Initial Segment (AIS), which is a segment with a high density of voltage-sensitive sodium channels and it is the spike initiate site in almost all types of neurons [Fried et al.(2009); Mainen et al.(1996)]. The sodium conductivity of the cell AIS has been shown in the histogram in Figure 3.8.

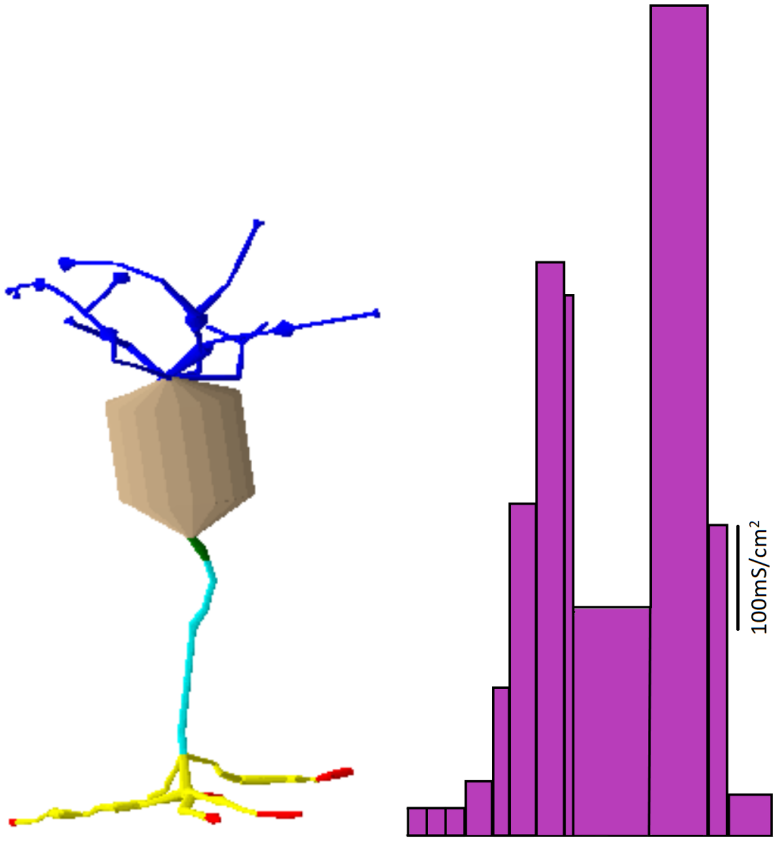

Figure 3.7: 3-D Model of DB4 (Left), the distribution of the sodium ion channels which amplify excitation and the values of this histogram were used as individual conductance parameters for sodium band comparments(Right). In the histogram a peak conductance value close to 1000 mS/cm^2 for voltage sensitive sodium channel type Nav1.1 playes an important role of all sodium ions when generating spikes.

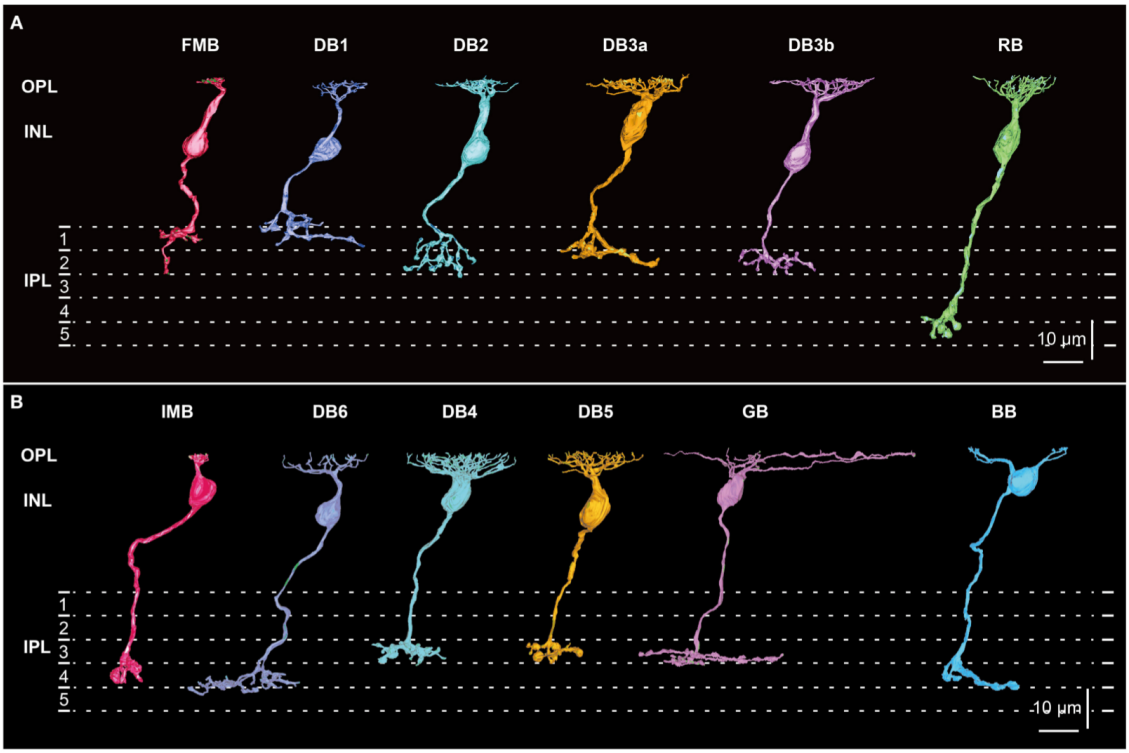

Figure 3.8: Morphology and stratication of FMB, DB1, DB2, DB3a, and DB3b types of OFF bipolar cells. FMB cell-1 and cell-6 (FMB-1 and FMB-6) are connected to M/L and S cones, respectively. Four cells (1-4) are displayed for each DB type. Each stratum of the IPL (1-5) is 6 μm thick. Strata 1-2 comprise the OFF sublamina [Tsukamoto et al.(2015)].

To give a comparison between a BC cell and two other different cells, in Table 3.3, the morphometric and sodium channel density of different parts of them has been shown.

Table 3.3: Morphometric and sodium channel density data of three different cells

	Bipolar Cell	**Ganglion Cell**	**Pyramidal Cell**
Dendrite $g_{Na}(mS/cm^2)$	0	25	8
Soma $g_{Na}(mS/cm^2)$**)**	0	80	8
Axon $g_{Na}(mS/cm^2)$	0	70	300
Sodium band $g_{Na}(mS/cm^2)$	350	400	420
Soma diameter (μm)	10.3	20	20
Sodium band diameter (μm)	0.5	2	1.22
Sodium band length (μm)	26	40	50
Distance between sodium band and soma (μm)	4.7	40	10
Main reference	[Puthusserry et al.(2013)]	[Rattay et al.(2014)]	[Rattay et al.(2012)]
Additional reference		[Sheasby et al.(1999), Jeng et al.(2011)]	[Mainen et al.(1996), Hu et al.(2009)]

Since Bipolar Cells have extremely short axons, therefore shorter sodium band and limited sodium channels, they can generate more spikelet rather than an action potential with a 100 mV amplitude [Rattay et al.(2017)]. However, the focus of this study is to find at what stimulus amplitude, shape and electrode position the BCs will respond with APs but this should be taken into account the corresponding APs have much lower amplitude than the amplitude that an AP has typically in other sensitive cells such as GCs or pyramid cells. To have an understanding of this specific APs, a definition of where an AP in this study has been counted will be given at the beginning of the Result chapter. For simulation purposes, the multi-compartment model and Backward Euler solver have been chosen for this investigation which was explained in more detail in the background chapter.

3.3.2 Morphometry of the cell

The BC model is based on the reconstructed 3-D morphology of a retinal DB4 cell from macaque and ion channel dynamic data from [Puthussery et al.(2013)]. To simplify the calculations, the soma of the cell was replaced by a sphere with the same surface as the real cell's soma. The Hodgkin-Huxley model has been used for all channels. Sodium channel Nav1.1 density distribution in the sodium band has a peak represented by $g_{Na} = 1000\ mS/cm^2$ shown in Figure 3.7. The kinetics of m, h, and s Nav1.1 gates were defined by $V_{half} = -27.2$, -60, -60 mV with slopes $z = 4.6$, 7.7, and 5.4 mV, respectively [Spampanato et al.(2004); Barela et al.(2006)]. The T-type Cav3.1 is assumed to be of constant density ($g_{Ca} = 2mS/cm^2$) in soma, dendrite, and axon hillock compartments. Its m and h gates are defined by $V_{half} = -57$, -81 mV and slopes $z = 6.2$ and 4 mV, respectively [Deleuze et al.(2012)]. The two applied potassium channels are fast and slow types. The fast type is located in sodium band with $g_K = 2mS/cm^2$ while the slow potassium channel is located at the soma, dendrite, and axon hillock with $g_K = 2.4\ mS/cm^2$. This conductance value was derived from the voltage clamp experiments in [Puthussery et al.(2013)].

The kinetics of potassium channels are based on the original Hodgkin-Huxley potassium channel but include a voltage offset and a tau rate which slows down the channel by the given factor. The fast potassium channel of the sodium band is shifted by 5 mV and has a tau rate of 5 which means 5 times slower than standard Hodgkin-Huxley potassium channel, while the slow channel has no voltage shift and tau rate of 8.

L-type Cav1.4 and HCN1 channels are located in terminals with densities 10^{-4} and 10^{-5} mS/cm^2 [Rattay et al.(2017)], respectively with kinetics used in [Wergniz & Rattay et al.(2016); Zhang et al.(2000)]. However, the L-type current conductivity may be essentially larger as investigated in [Protti et al. (1998)]. He reported the kinetic and pharmacological properties of I_{Ca} were very similar for recordings obtained from the soma and the presynaptic terminals. Leak current conductance $g_L = 0.033\ mS/cm^2$ and membrane capacitance C_m of 1 $\mu F/cm^2$ are taken from [Puthussery et al.(2013)]. For all of the calculations temperature coefficients were used to simulate the dynamics at 31°C [Rattay et al.(2002)]. In the following section, all presented channels with their dynamics are explained in detail.

Kinetics of the channels

- Sodium channel $Na_{V1.1}$ with the g_{Na} shown in Figure 3.7

$$\begin{aligned} G_{Na_{V1.1}} &= g_{Na} \times m_{Na}^3 \times h_{Na} \times s_{Na} \\ I_{Na} &= G_{Na_{V1.1}} \times (V - E_{Na}) \\ with\ E_{Na} &= 50.0mV \end{aligned} \tag{3.15}$$

– kinetics of activation [Puthussery et al.(2013); Aradi et al.(2002)]

$$\begin{aligned} V_{1/2} &= -57mV \\ Z &= 6.2mV \\ m_\infty(V) &= \frac{1}{(1+exp(-(V-V_{1/2})/6.2)} \\ \tau_m &= 0.612 + \frac{1}{exp(-(V+132.)/16.7) + exp(+(V+16.8)/18.2)} \end{aligned} \tag{3.16}$$

– kinetics of fast inactivation [Spampanato et al.(2004)]

$$\begin{aligned} V_{1/2} &= -60.mV \\ Z &= 7.7mV \\ h_\infty(V) &= \frac{1}{(1+exp(-(V-V_{1/2})/7.7)} \end{aligned} \tag{3.17}$$

– kinetics of slow inactivation [Spampanato et al.(2004)]

$$\begin{aligned} V_{1/2} &= -60mV \\ Z &= 5.4mV \\ s_\infty(V) &= \frac{1}{(1+exp(+(V-V_{1/2})/5.4)} \\ \tau_s &= 1000 \times (106.7 \times exp(-0.5 \times ((V+52.7)/18.3)^2)) \end{aligned} \tag{3.18}$$

- T-type Calcium channel $Ca_{V3.1}$ with $g_{Ca} = 2mS/cm^2$ presented in terminals.

$$\begin{aligned} G_{Ca_{V3.1}} &= g_{Ca} \times m_{Ca}^2 \times h_{Ca} \\ I_{CaV3.1} &= G_{Ca_{V3.1}} \times (V - E_{Ca}) \\ &with\ E_{Ca} = 20mV \end{aligned} \tag{3.19}$$

– kinetics of activation [Deleuze et al.(2012)]

$$
\begin{aligned}
&V_{1/2} = -57mV \\
&Z = 6.2mV \\
&m_\infty(V) = \frac{1}{(1 + exp(-(V - V_{1/2})/6.2)} \\
&\tau_m = 0.612 + \frac{1}{exp(-(V + 132.)/16.7) + exp(+(V + 16.8)/18.2)}
\end{aligned}
\tag{3.20}
$$

– kinetics of inactivation

$$
\begin{aligned}
&V_{1/2} = -81mV \\
&Z = 4mV \\
&h_\infty(V) = \frac{1}{1 + exp(+(V - V_{1/2})/4)} \\
&\tau_\infty(V) = 28 + exp(-(V + 22)/10.5)\ for\ V \geq -81mV \\
&\tau_\infty(V) = exp((V + 467.)/66.6)\ for\ V < -81mV
\end{aligned}
\tag{3.21}
$$

- L-type Calcium channel $Ca_{V1.4}$ with $g_{Ca} = 10^{-4} mS/cm^2$ presented in terminals.

$$
\begin{aligned}
&G_{Ca} = g_{Ca} \times c^3 \\
&I_{Ca} = G_{Ca} \times (V - E_{Ca}) \\
&with\ E_{Ca} = 120mV
\end{aligned}
\tag{3.22}
$$

– Dynamic of the channel with variable gate c [Wergniz & Rattay et al.(2016)]

$$\begin{aligned}
&\alpha_c(V) = -0.3 \times \frac{(V+70)}{exp(-0.1 \times (V+70)) - 1} \; for \; V < -70mV \; or \; V > -70mV \\
&\alpha_c(V) = 2.999249 \; for \; V = -70mV \\
&\beta_c(V) = 10 \times exp(\frac{-(V+38)}{9}) \\
&c_\infty(V) = \frac{\alpha_c}{\alpha_c + \beta_c} \\
&\tau_c(V) = \frac{1}{\alpha_c + \beta_c}
\end{aligned} \tag{3.23}$$

- Hyperpolarization-activated cyclic nucleotide-gated (HCN) is a gate presents in the plasma membrane of heart and brain cells. However in this cell with $g_{HCN} = 10^{-5} mS/cm^2$ and gate located in terminals [Zhang et al.(2000)].

$$\begin{aligned}
&G_{HCN} = g_{HCN} \times y \\
&I_{HCN} = G_{HCN} \times (V - E_{HCN}) \\
&with \; E_{HCN} = -40mV
\end{aligned} \tag{3.24}$$

– Dynamics of the channel with variable gate y

$$\begin{aligned}
&\alpha_y(V) = exp(\frac{-(V+78.91)}{26.62}) \\
&\beta_y(V) = exp(\frac{(V+75.13)}{21.25}) \\
&y_\infty(V) = \frac{\alpha_y}{\alpha_y + \beta_y} \\
&\tau_y(V) = \frac{1}{\alpha_y + \beta_y}
\end{aligned} \tag{3.25}$$

- The fast potassium channel with $g_K = 2mS/cm^2$ located at sodium band [Hodgkin & Huxley et al.(1952b)]

  – Dynamics of the channel

$$
\begin{aligned}
&V_{offset} = 5mV \\
&\tau_{rate} = 5 \\
&G_K = g_K \times n^4 \\
&I_{Kslow} = G_K \times (V - E_K) \\
&\alpha_n(V) = 0.1 \times (-0.1) \times \frac{(V - V_{offset} + 55)}{exp(-0.1 \times (V - V_{offset} + 55)) - 1} \times \frac{1}{\tau_{rate}} \\
&\beta_n(V) = 0.125 \times exp(\frac{(V - V_{offset} + 65)}{-80}) \times \frac{1}{\tau_{rate}} \\
&n_\infty(V) = \frac{\alpha_n}{\alpha_n + \beta_n} \\
&\tau_n(V) = \frac{1}{\alpha_n + \beta_n}
\end{aligned}
\tag{3.26}
$$

- The slow potassium channel with $g_K = 2.4mS/cm^2$ located at soma, dendrite and axon hillock [Hodgkin & Huxley et al.(1952b)].

  – Dynamics of the channel

$$
\begin{aligned}
&V_{offset} = 0mV \\
&\tau_{rate} = 8ms \\
&G_K = g_K \times n^4 \\
&I_{Kslow} = G_K \times (V - E_K) \\
&\alpha_n(V) = 0.1 \times (-0.1) \times \frac{(V - V_{offset} + 55)}{exp(-0.1 \times (V - V_{offset} + 55)) - 1} \times \frac{1}{\tau_{rate}} \\
&\beta_n(V) = 0.125 \times exp(\frac{(V - V_{offset} + 65)}{-80}) \times \frac{1}{\tau_{rate}} \\
&n_\infty(V) = \frac{\alpha_n}{\alpha_n + \beta_n} \\
&\tau_n(V) = \frac{1}{\alpha_n + \beta_n}
\end{aligned}
\tag{3.27}
$$

before final calculation, the temperature dependency of all functions needs to be considered according to the following rule:

$$
\tau'_x = \tau_x \times Q_{10}^{-(T-T')/10} \tag{3.28}
$$

Where Q_{10} is the experimentally determined change of time constants for a 10 degree difference in temperature, T is the stimulation temperature which is set at 31°C and T' is an individual temperature value at which the empirical functions and dynamics have been calculated. All temperature parameters for the six present channel types have been shown in Table 3.4.

Table 3.4: Temperature Parameters

Channel Type	Q_{10}	T'
$Na_{V1.1}$	Q_{10_m}= 2.2 Q_{10_h}= 2.9 Q_{10_s}= 2.9	20
T-type Calcium channel	Q_{10_m}= 5 Q_{10_h}= 3	24
L-type Calcium channel	1	10
HCN1	1	37
Fast potassium channel	2	6.3
Slow potassium channel	2	6.3

So finally, the ionic current equation should be written as:

$$I_{ion} = I_{Na} + I_{Ca_{V3.1}} + I_{Ca} + I_{HCN} + I_{Kslow} + I_{Kfast} + I_L \tag{3.29}$$

Chapter 4

Results

In this chapter, some intra and extracellular stimulation of the cell have been done through the computer simulations and the results have been demonstrated and discussed. At the end of the chapter, a Gaussian noise has been added to the model. Finally, the cell has been stimulated with the included noise channel, and the result has been compared.

4.1 Intracellular stimulation

Over the past 70 years, many researchers tried to understand the nervous system in two parallel levels. On the one hand, scientists are always trying to achieve a better understanding of the circuit properties of the nervous system and how neurons are connected to process information and communicate in various behaviours. On the other hand, there have been many efforts and requirements to understand the function of an individual neuron itself and the biophysical mechanisms of its electrical activities [Byrne et al.(1981)]. Parallel studies have shown the necessity of the exact controlling of the membrane potential for instance for synaptic activities. Therefore the intracellular stimulation was established to analyse the behaviour of a single cell and allows to control it. First progresses in this area was due to the development of the

glass capillary microelectrode by Ling and Gerard [Ling and Gerard et al.(1949)]. This made it possible to monitor the intracellular potential of individual neurons and to record their response to an input.

The most reliable technique for intracellular stimulation is the voltage clamp technique, briefly explained in section 2.2. This study has provided different anodic currents injected in four positions of a DB4 to find an appropriate amplitude and waveform of an injected current for stimulation purposes, this study has provided different anodic currents injected in four positions of a DB4. Regarding this goal, in the next steps, some substantial test results are discussed. These steps are done with considering the frequency factor and observing whether the cell responses will change or not.

4.1.1 How to define an action potential

Before starting the result section, a short definition of where in this study an AP is counted needs to be given. Since the investigated cell is a BC, a spike which is attributed to an AP differs from the one in other cells. Usually, an AP has an increment of about 100 mV, but this is not the case in BC cells. In order to find an appropriate threshold to count APs, the cell has been stimulated with a virtual intracellular electrode positioned in the soma. The simulation was run 25 times, with an anodic rectangular pulse current with a duration of 100 ms, an amplitude changing from 0 to 50 pA and the membrane voltage recorded in the injected site. As shown in Figure 4.1, the maximum voltage which is very similar to an AP in soma is less than 10 mV or has even minus values shown in Figure 4.2.
In this investigation, the position of the electrode for injected current and recording V has been considered for four regions soma, sodium band, dendrite and terminal. Therefore a threshold to recognise an AP might not be the same in all the cases. Hence, four different conditions will be discussed separately in the following sections.

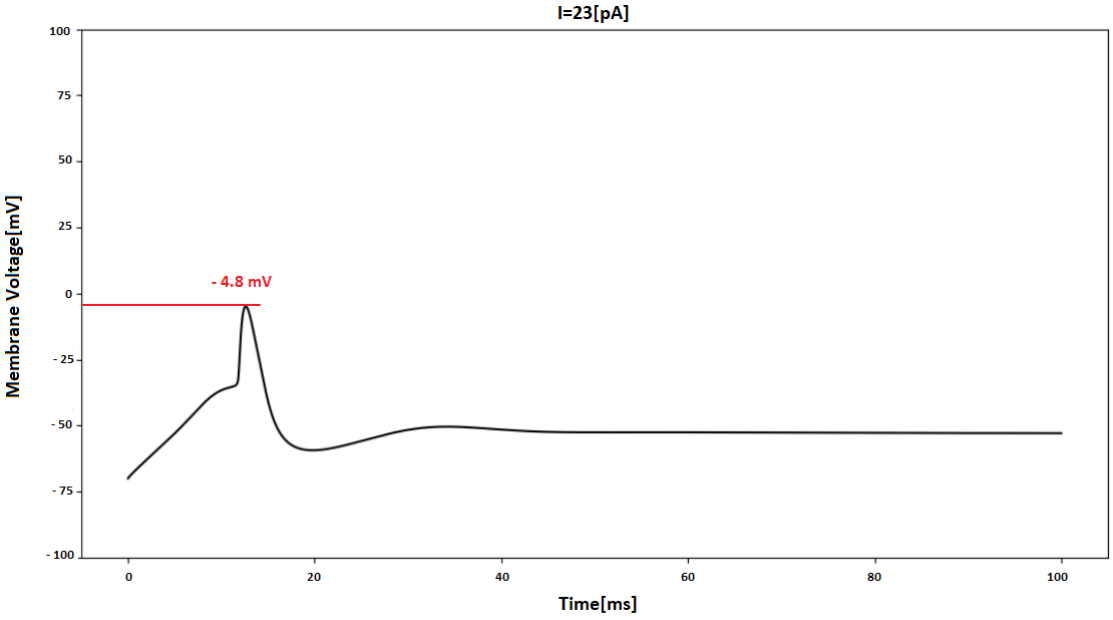

Figure 4.1: Appearance of an action potential at amplitude 23 pA and the maximum membrane voltage at -4.8 mV

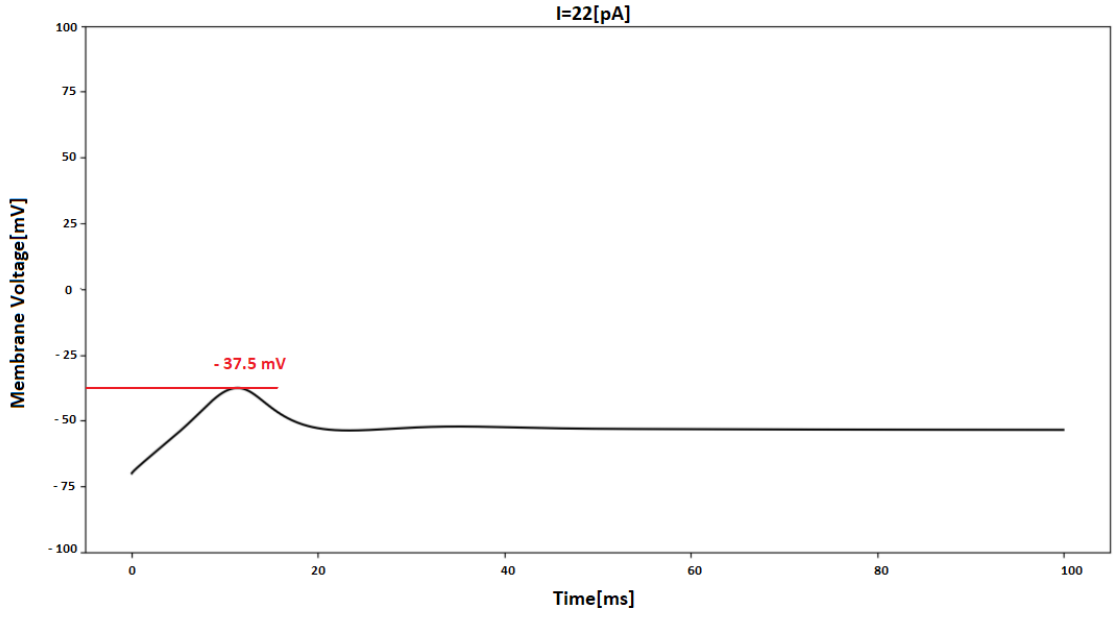

Figure 4.2: Stimulating with I=22 pA with membrane potential peak at -37.5 mV

- **Soma injection:**

  There is a gap between potential values of -40 mV and about -5 mV, which means after increasing the current from 22 pA the membrane voltage will bounce from -40 to -5 mV and an AP is occurred. Therefore in this study, a part of this gap value which is about -30 mV, has been chosen as the defined threshold of APs. However, this should be mentioned that this value is entirely different from the membrane voltage threshold of an AP.

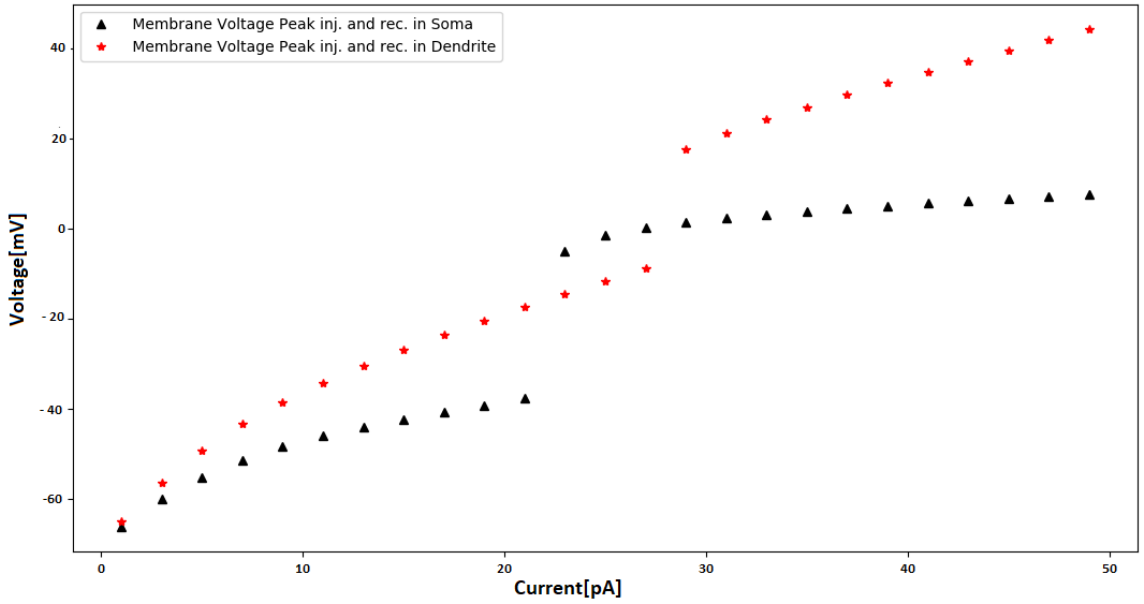

Figure 4.3: 25 times run of stimulating in the soma and dendrite with current amplitude from 0 to 50 pA, membrane voltage recorded in both soma and dendrite.

- **Dendrite injection:**

  Dendrite injection is shown in Figure 4.3 with red stars. In this case, the threshold has been chosen at 0 mV. Despite dendritic potential importance in neuronal function, direct experimental evidence on electrical signalling in dendritic spines is lacking as their small size makes them inaccessible to standard electro-physiological techniques. Because the vast majority of excitatory synaptic input in many regions is made directly onto dendrites, understanding their physiology and function is critical [Palmer et al.(2009)]. Nevertheless, it has been proved that the local voltage thresholds for dendritic spike

initiation are usually higher than that of action potential initiation in the axon; therefore, spike initiation usually requires a strong input [Haeusser et al.(2000)]. This is also shown in Figure 4.3 that the spike initiation in dendrites needs higher amplitude, which is about 28 pA, in contrast to the other parts of the cell.

- **Terminal and sodium band injection:** As shown in Figure 4.4, in both positions the cell behaviour is found almost similar. Therefore, the threshold has been chosen at about -10 mV. The cell begins to respond with an AP at about 19 pA in case of a rectangular anodic pulse stimulus, which is smaller than previous cases.

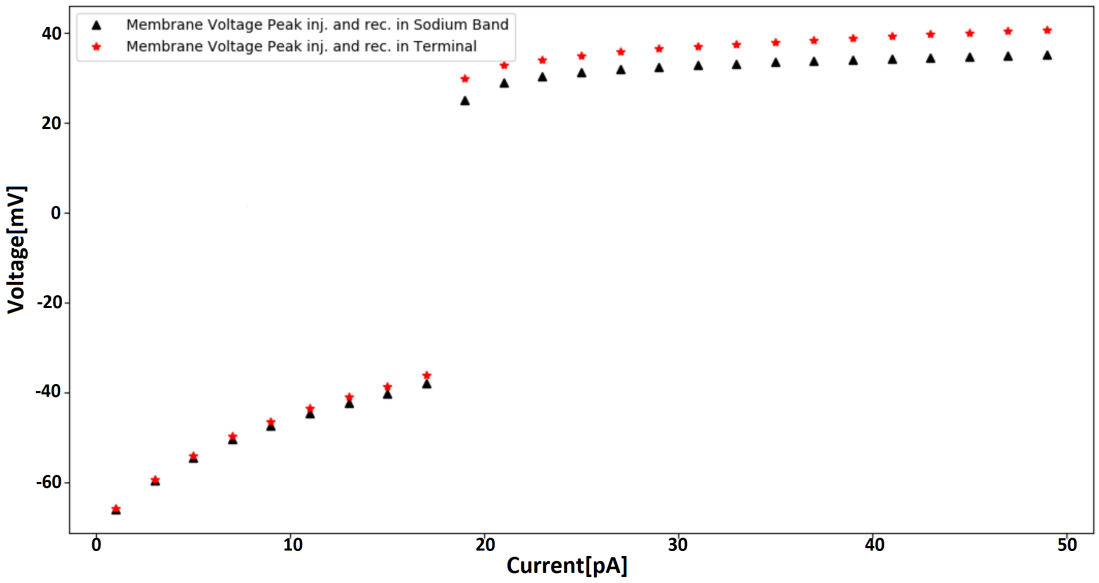

Figure 4.4: 25 times run of stimulating in the sodium band and terminal with current amplitude from 0 to 50 pA, membrane voltage recorded in both sodium band and terminal.

4.1.2 Transmembrane currents

Investigating the currents of different segments helps to understand when and where currents through the ion channels in the cell membrane are involved. The current contribution is helpful to study the behaviour of a BC and the currents contribution to the cell activations.

In this section, transmembrane currents, shown in the following figures, include five different currents originated from five type of ion channels which are distributed in the cell compartments. The currents are recorded in soma Figure 4.5, in sodium band Figure 4.6, in terminal Figure 4.7, in dendrite Figure 4.8, and finally the total currents of all 117 compartments are shown in Figure 4.9. All responses in this section are due to an intracellular stimulation by a single rectangular pulse of duration 10 ms, having once a subthreshold amplitude of 20pA and once a suprathreshold amplitude of 30 pA.

Figures show that L-type and T-type calcium channels, as well as the slow potassium channel, are activated before sodium channel. In case of 20pA stimulus, the fast potassium channel is activated before the sodium channel while by increasing the amplitude to 30 pA both channels are activated almost simultaneously. L-type calcium channel has the lowest contribution while the sodium channel has the highest contribution to the cell membrane currents.

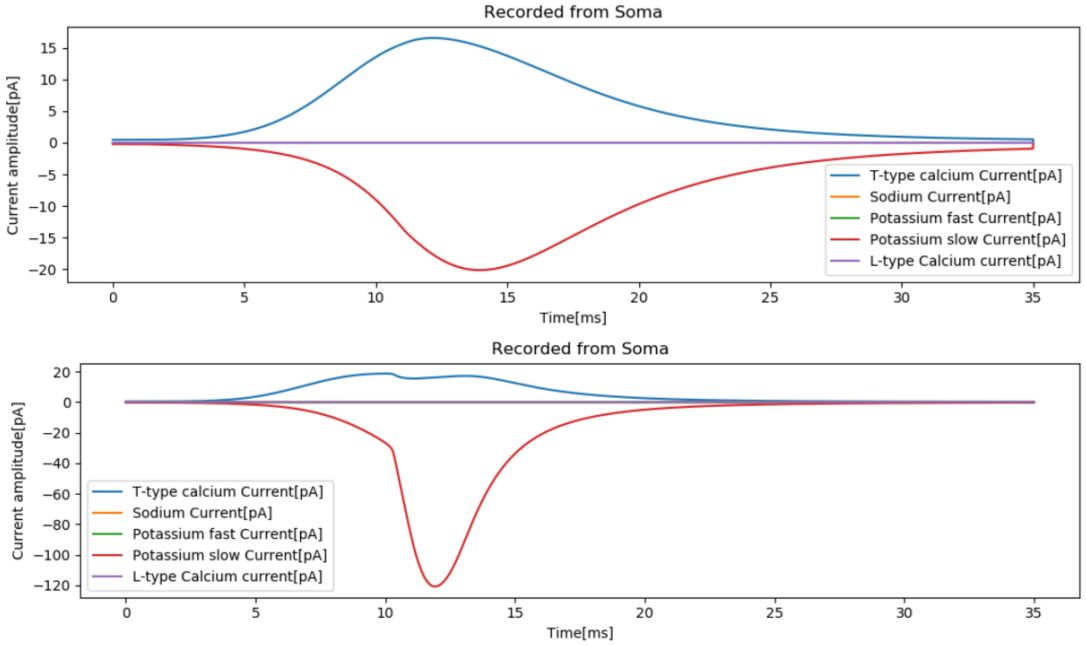

Figure 4.5: Transmembrane currents in case of: A) Subthreshold of the amplitude of 20 pA with the coincidence of L-type, T-type calcium and slow potassium currents. B) Suprathreshold of the amplitude of 30 pA with the coincidence of L-type and T-type calcium and slow potassium currents. In both cases the injection site was dendrite and the transmembrane currents are recorded in soma.

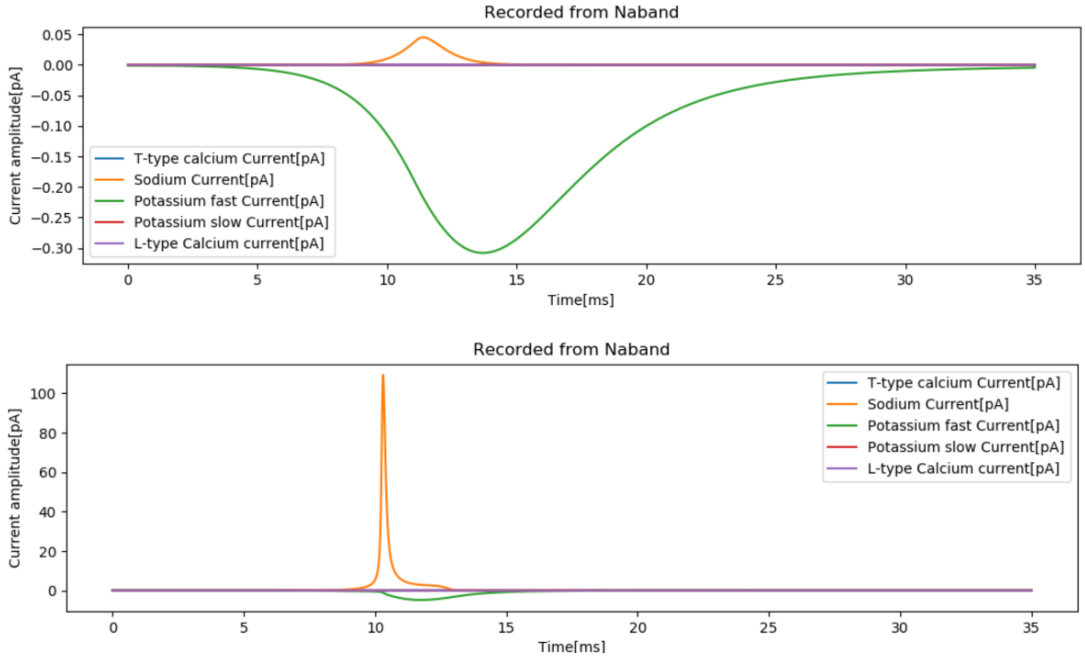

Figure 4.6: Transmembrane currents in case of: A) Subthreshold of the amplitude of 20 pA with the coincidence of L-type, T-type calcium and slow potassium currents. B) Suprathreshold of the amplitude of 30 pA with the coincidence of L-type and T-type calcium and slow potassium currents. In both cases the injection site was dendrite and the transmembrane currents are recorded in sodium band.

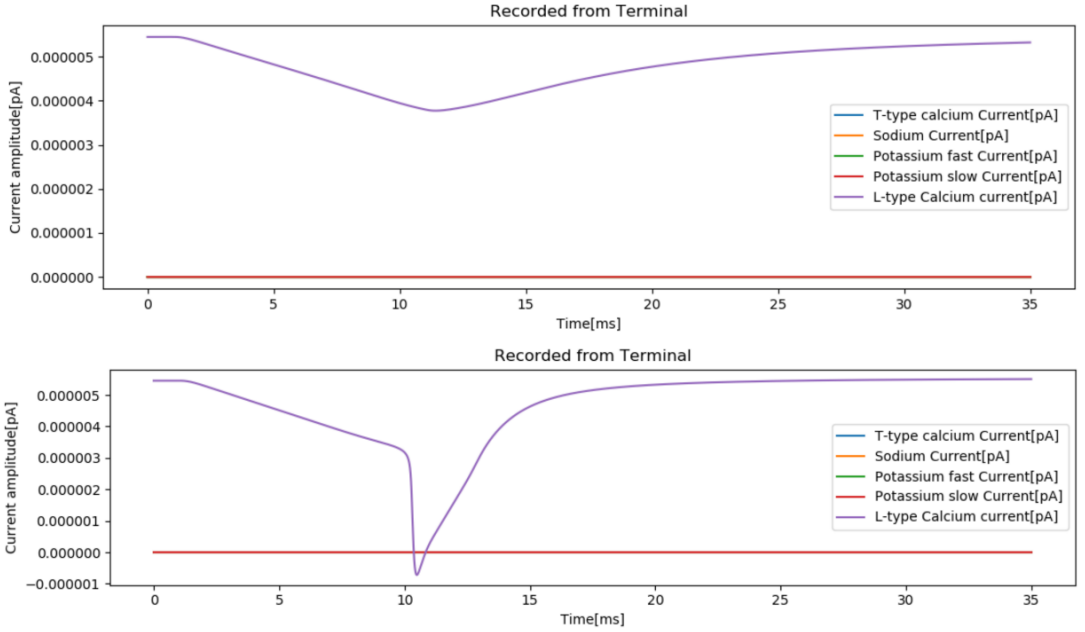

Figure 4.7: Transmembrane currents in case of: A) Subthreshold of the amplitude of 20 pA with the coincidence of all currents except slow potassium current. B) Suprathreshold of the amplitude of 30 pA again with the coincidence of all currents except slow potassium current. In both cases the injection site was dendrite and the transmembrane currents are recorded in terminal.

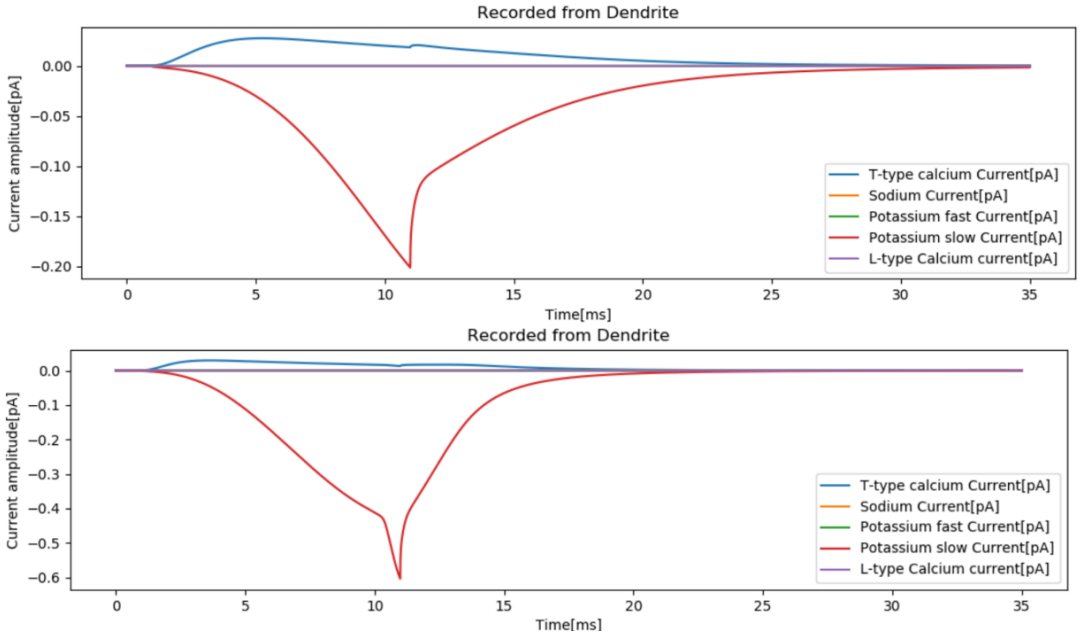

Figure 4.8: Transmembrane currents in case of: A) Subthreshold of the amplitude of 20 pA with the coincidence of L-type and sodium and fast potassium currents. B) Suprathreshold of the amplitude of 30 pA again with the coincidence of L-type and sodium and fast potassium currents. In both cases the injection site was dendrite and the transmembrane currents are recorded in dendrite.

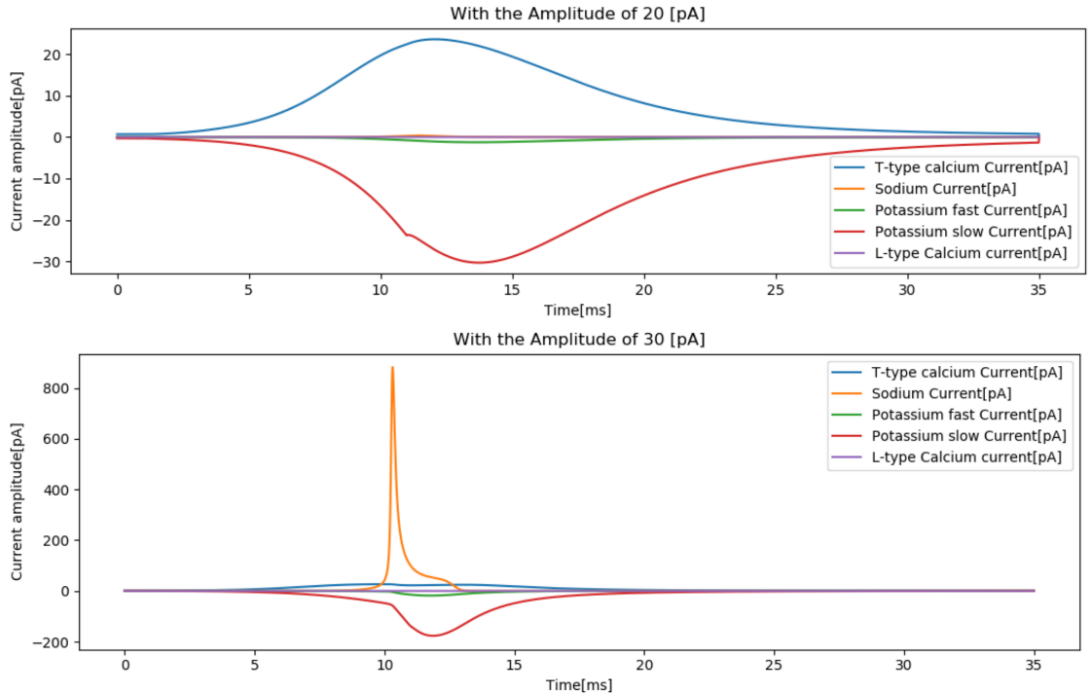

Figure 4.9: Transmembrane currents in case of: A) Subthreshold of the amplitude of 20 pA with the coincidence of L-type and sodium currents and a B) Suprathreshold of the amplitude of 30 pA. In both cases the injection site was dendrite and the transmembrane currents present the total currents of all compartments.

4.1.3 Anodic rectangular pulses

In this section, some anodic rectangular currents have been injected in different parts of the DB4 cell, and critical amplitudes are discussed. The amplitude of the injected current differs from 20 to 50 pA at the frequency range 1 Hz to 100 Hz for the stimulation time of 500 ms.

- **Anodic rectangular pulses with the amplitude of 20 pA**

  20 pA could be a critical value, since in this amplitude the position of the electrode should be taken into account. A 20 pA stimulus can excite the cell to respond with APs, but it is not always the case. Regarding previous discussions, a 20 pA stimulus can generate AP when the electrode is positioned in either sodium band or terminals but neither in soma nor dendrite. As shown in Figure 4.10, at sodium band and terminal, the cell generates APs within the frequency range of 1 Hz to about 40 Hz, and even in some frequencies, more than one AP will be generated. However, 20 pA might not be enough to excite this cell.

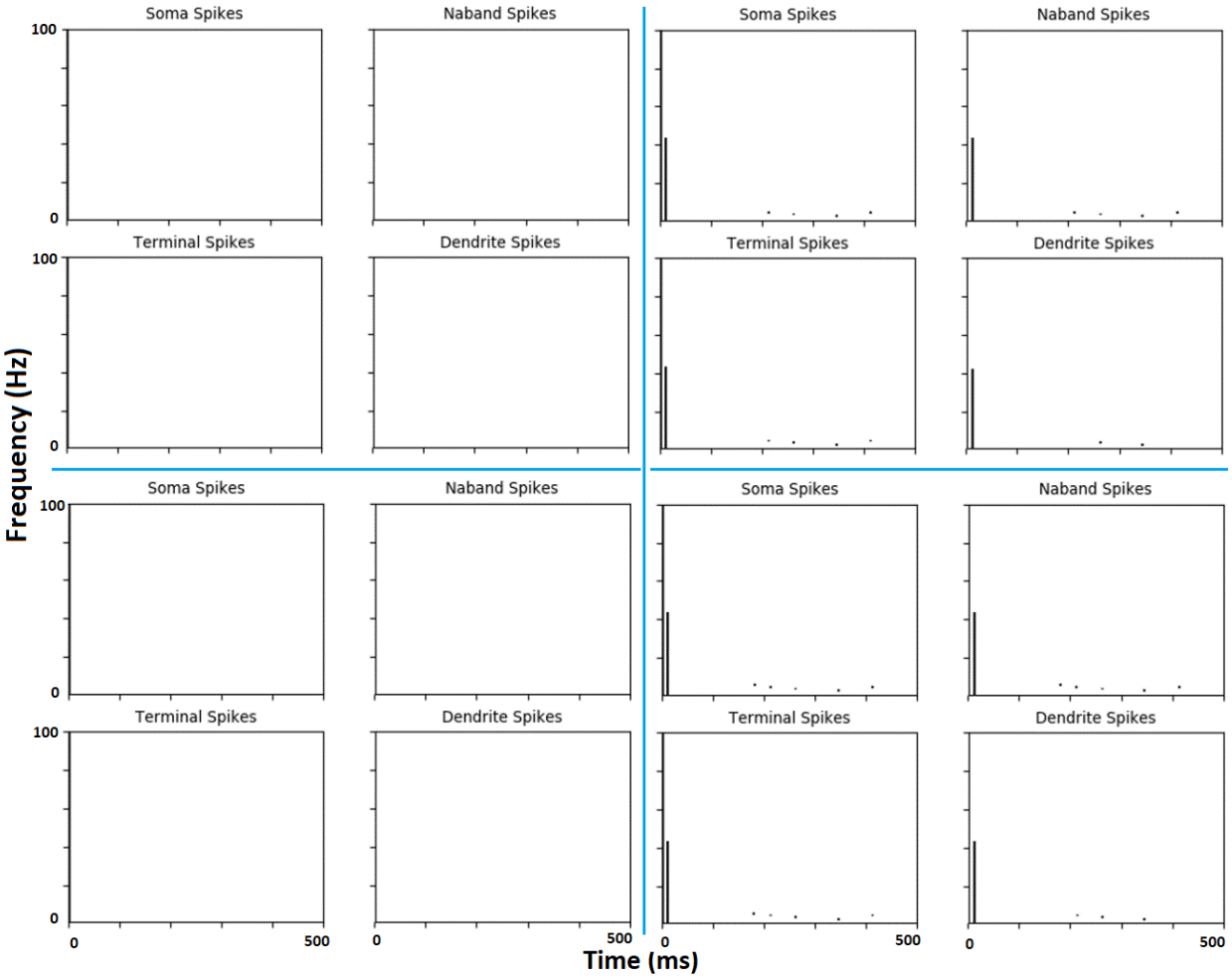

Figure 4.10: Top left: injection in dendrite, Top right: injection in sodium band, Bottom right: injection in terminal, Bottom left: injection in soma. In case of soma and dendrite injections, no AP is produced. Some APs recorded from dendrite may not have been recorded because their amplitudes are below the defined amplitude.

- **Anodic rectangular pulses with the amplitude of 25 pA**

  An amplitude of 25 pA can be more reasonable to stimulate the cell. It can be excitable if injected in three positions but not in the case of dendrites. The two appropriate positions, in this case, might be the sodium band and soma. Furthermore, an adequate frequency range to excite the cell with this amplitude can be the values smaller than 20 Hz, though more energy is needed to generate more APs.

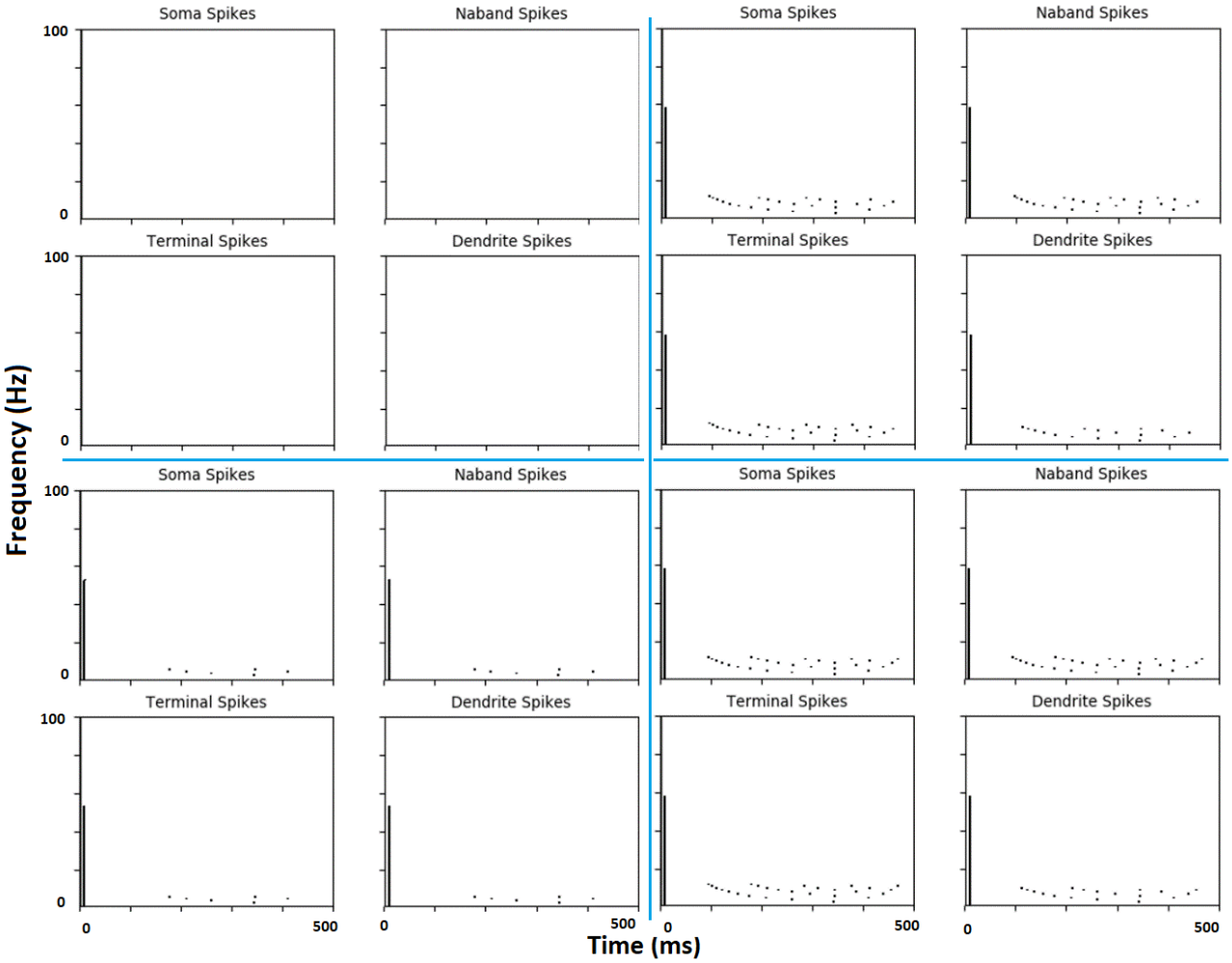

Figure 4.11: Top left: injection in dendrite, no AP occurred, Top right: injection in sodium band, Bottom right: injection in terminal, Bottom left: injection in soma

- **Anodic rectangular pulses with the amplitude of 30 pA**

  In an amplitude of 30 pA, the electrode position still matters, and the proper frequency range might be within 10 to 40 Hz. However, dendrite and terminal still need more energy to generate more APs.

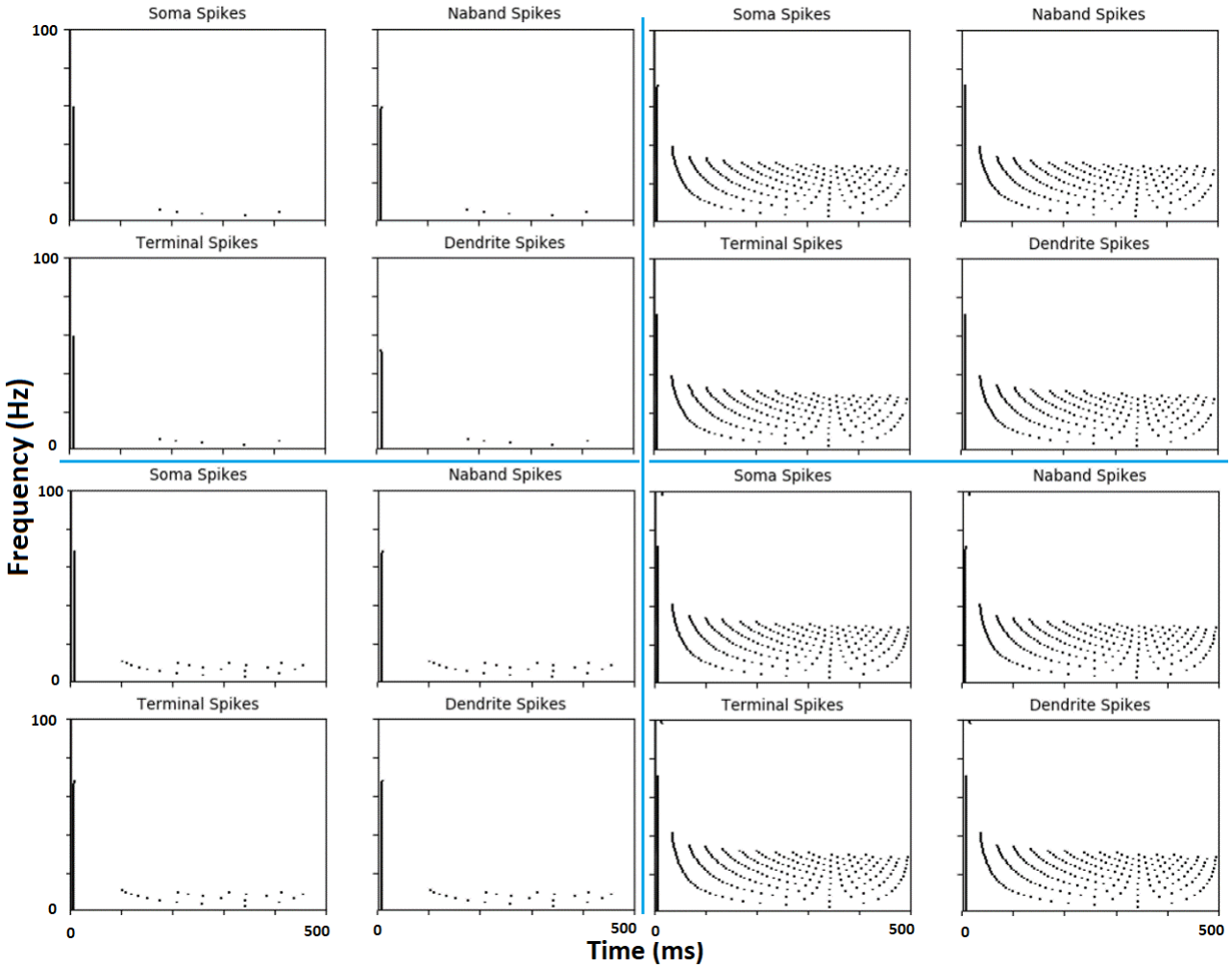

Figure 4.12: Top left: injection in dendrite, Top right: injection in sodium band, Bottom right: injection in terminal, Bottom left: injection in soma

- **Anodic rectangular pulses with the amplitude of 50 pA**

  50 pA can be a suitable amplitude for this simulated cell and to generate the maximum APs best position might be again either in soma or sodium band. A suitable frequency, therefore, might be between 20 to 80 Hz. However, this range is smaller in case of the terminal injection.

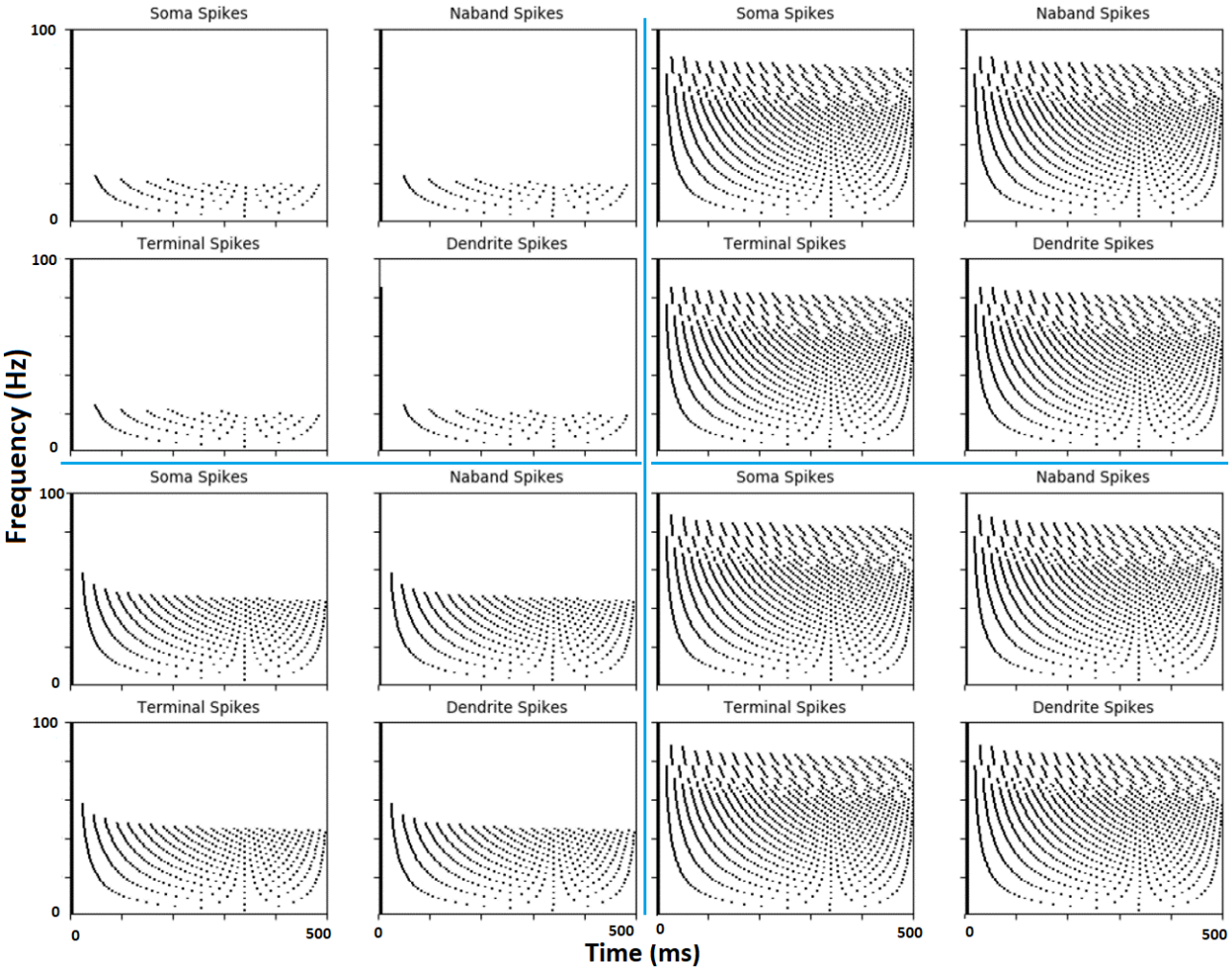

Figure 4.13: Top left: injection in dendrite, Top right: injection in sodium band, Bottom right: injection in terminal, Bottom left: injection in soma

4.1.4 Anodic sinusoidal pulses

In this section, the cell has been stimulated through sinusoidal pulses with two different amplitudes, 30 and 50 pA in range of frequency 0 to 100 Hz to assess which position and what amplitude is a reasonable choice in contrast to a rectangular pulse. However, the amplitude, in which the cell begins to respond is larger than the one in the rectangular case. A reason for that might be because the area under a sinusoidal curve is smaller than the area under a rectangular curve with the same amplitude and injection time. Therefore more energy or more amplitude is needed for a sinusoidal current to provoke the cell response.

- **Anodic sinusoidal pulses with the amplitude of 30 pA**

  An amplitude of 30 pA is still not enough in case of dendrite injection. This amplitude may not be a suitable amplitude for this shape of the pulse to stimulate the cell as shown in Figure 4.14.

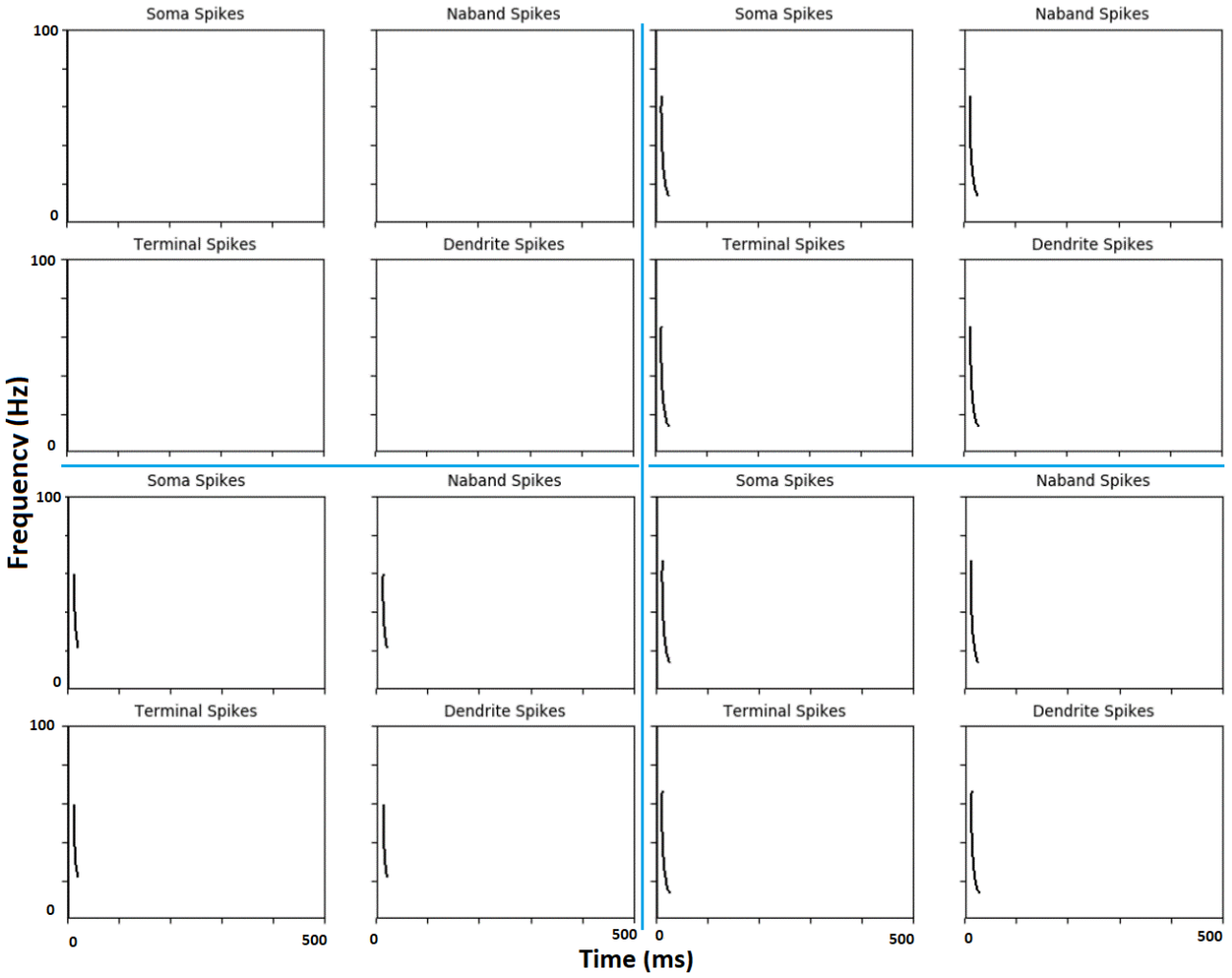

Figure 4.14: Top left: injection in dendrite, no AP is occurred, Top right: injection in sodium band, Bottom right: injection in terminal, Bottom left: injection in soma

- **Anodic sinusoidal pulses with the amplitude of 50 pA**

  50 pA might be more suitable if the electrode is positioned either in the soma or sodium band. Therefore, in this case, even more amplitude is needed to obtain a proper result.

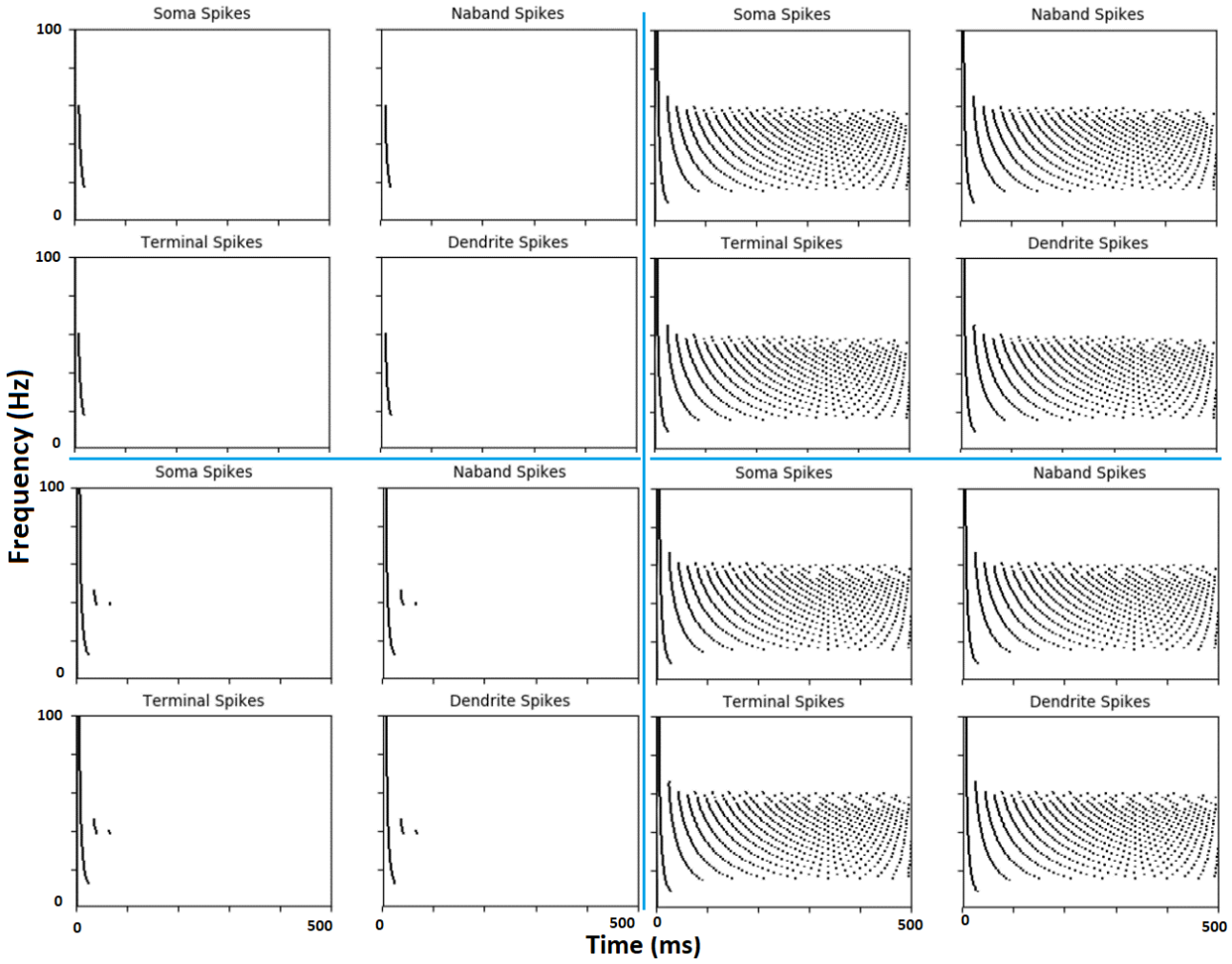

Figure 4.15: Top left: injection in dendrite, Top right: injection in sodium band, Bottom right: injection in terminal, Bottom left: injection in soma

4.1.5 Summary

Since APs travel through the whole cell, they should be recorded in all compartments with the same number , but they may not have the same amplitudes. In some cases, the number of APs recorded in dendrite may not be equal to the other three record sites. This is because of the smaller amplitudes of the APs at the dendrite, since dendrite is the remotest site, thus some APs may occur under the defined threshold. As a result, the under threshold APs are not recorded here. In all previous cases, dendritic and somatic injections need stronger amplitudes to produce the same number of APs compared to the other two injection sites, sodium band and terminal. One reason for that is because of the distance, over which signals should travel until they arrive at the AP initiation site, sodium band and due to the intracellular resistivity, the longer the distance is, the more the amplitude reduces. The other reason is the small ratio of (surface of sodium-band)/(surface of soma), which attenuates the signal travelling to soma and dendrite. In case of rectangular pulses until 25 pA and in case of sinusoidal pulses until 30 pA there is still not enough energy to provoke the cell at any site. Accordingly, at these and smaller amplitudes, considering the injection site is essential.

4.2 Extracellular stimulation

Extracellular stimulation of nerve cells in a tissue is a classical technique in brain research and a fundamental tool in neuroprosthesis. The electrical current that originates at an electrode creates a gradient of extracellular electrical potential such that an action potential may be elicited. In recent years, particular attention was given to the extracellular stimulation. Questions considered were: Which part of a neuron is responsible for excitation? What is the role of anodic and cathodic current on attached and non-attached parts of the membrane? Or even the location of the electrode [Garcia et al.(2005); Merabet et al.(2005)].

For extracellular stimulation, the extracellular potential is given by the applied electric field. Depending on the electrode position related to a target neuron and the electrical properties of the cell, an extracellular stimulus causes depolarised regions and hyperpolarised regions of different strength along the neuron at the same time. The depolarising and hyperpolarising forces are independent of any active mechanisms of the cell, and they are just caused by the passive behaviour of a cell inside an electric field. When a stimulating square pulse establishes a time-invariant extracellular potential along the surface of the cell, the electric forces inside the cell tries to balance out the intracellular potential which is affected by the stimulus, too [Rattay et al.(2014)].

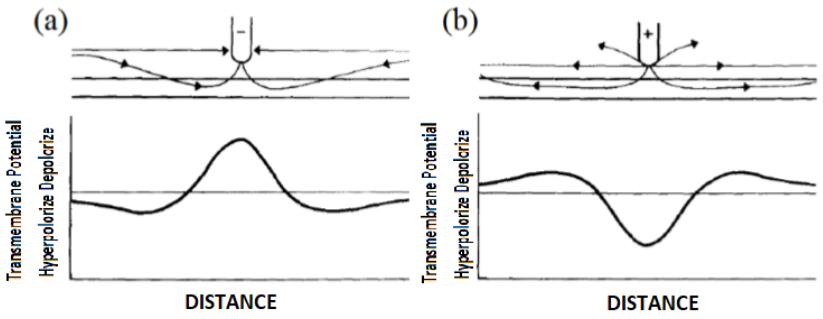

Figure 4.16: (a) Cathodic stimulation vs (b) Anodic stimulation

This section presents a numerical method (Backward Euler) to compute the effects of an electric field produced by a virtual electrode positioned on a 17.4 μm distance to the cell axis, below the dendritic edge. To model extracellular stimulation I_{ext} in Equation 4.2 is equal to an injected current into each compartment can be expressed by the following term [Rattay et al.(1999)]:

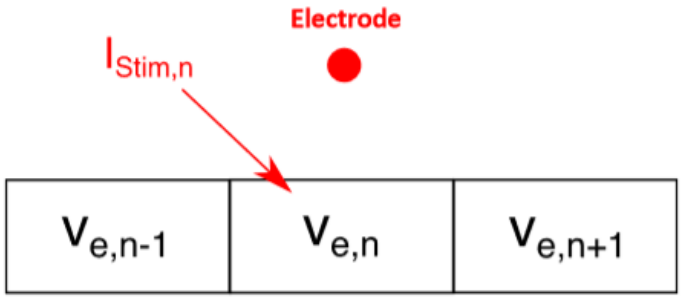

Figure 4.17: n compartment model with an external electrode

$$I_{stim_n} = \frac{(V_{e_n} - V_{e_{n-1}})}{(R_n/2 + R_{n-1}/2)} + \frac{(V_{e_n} - V_{e_{n+1}})}{(R_n/2 + R_{n+1}/2)} + ... \tag{4.1}$$

With $\frac{R}{2}$ denoting the half intracellular resistance of each compartment,V_{en} presenting for extracellular potentials at the compartment centres. To calculate external potentials, the electrode

is assumed a point source within a homogeneous medium. In this case, isopotentials are spheres and V_{ext} (in mV) can be calculated with:

$$V_{ext} = \frac{\rho_{ext} \times I_{ext}}{4 \times r \times \pi} \tag{4.2}$$

With r (in cm) being the Euclidean distance from the electrode (the distances between mid-points and electrode positions which is shown in method section), $\rho_{ext}(k\Omega cm)$ being the resistivity of the extracellular medium and the applied current of $Iext(\mu A)$ [Mcneal et al.(1976)]. ρ_{ext} is set to 1 $k\Omega cm$ in all simulations.

Again the simulations run for four positions to record, and it needs to define an individual threshold for each case to count APs. In the following figures, two examples are shown with the same frequency stimulus and the same amplitude with once anodic and once cathodic current. However, in order to get the same result, the stronger amplitude is needed in case of cathodic stimulation.

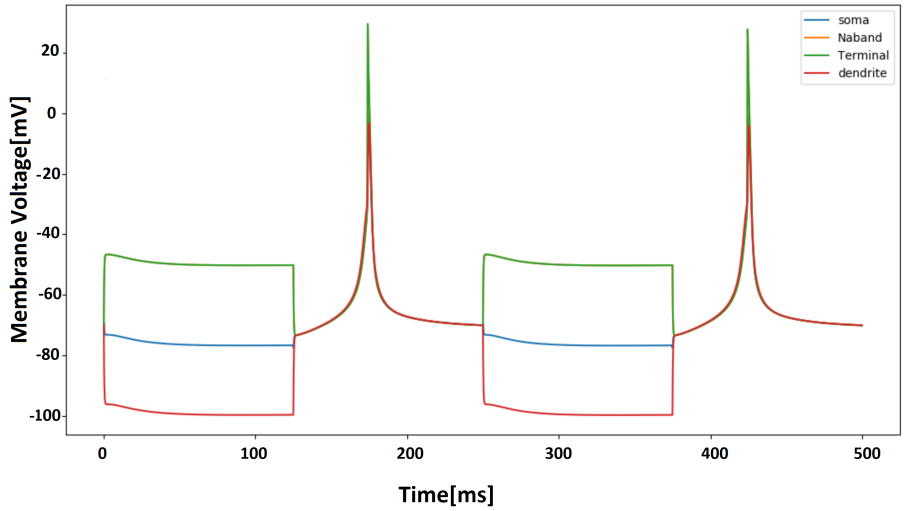

Figure 4.18: I=5 μA, for 500 ms stimulation, frequency= 3 Hz. At the AP regions, soma and dendrite are coincident while terminal, and sodium band are entirely coincident.

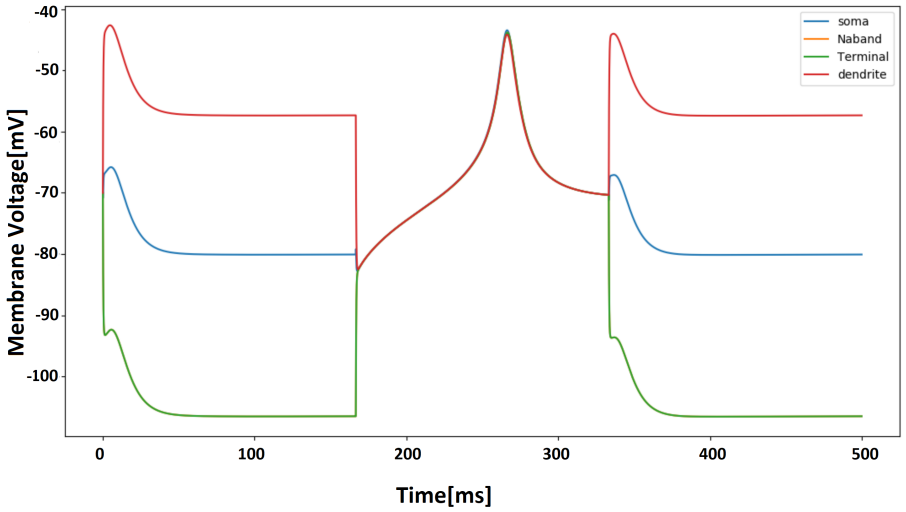

Figure 4.19: $I = -5\mu A$, for 500 ms stimulation, frequency= 3 Hz. At the spikelet region, soma and dendrite are coincident while terminal, and sodium band are entirely coincident.

In this section, the cell stimulation with three different anodic and cathodic amplitudes are shown to compare the effects of stimulus on different parts of the cell. However, this should be mentioned that in this investigation, the defined threshold for dendrites is changed to about -40 mV which is not any more similar to an AP but more similar to a spikelet.

In case of anodic stimulus, with increasing the amplitude, more APs are generated in each part of the cell except the dendrite. In case of cathodic stimulus, almost every part of the cell still needs stronger stimulus except the dendrites which are generating more spikelets, because with changing the polarity the most hyperpolarised dendrite become the most depolarised part of the cell and reach the -40 mv threshold. This fact is demonstrated in Figure 4.19 and Figure 4.20.

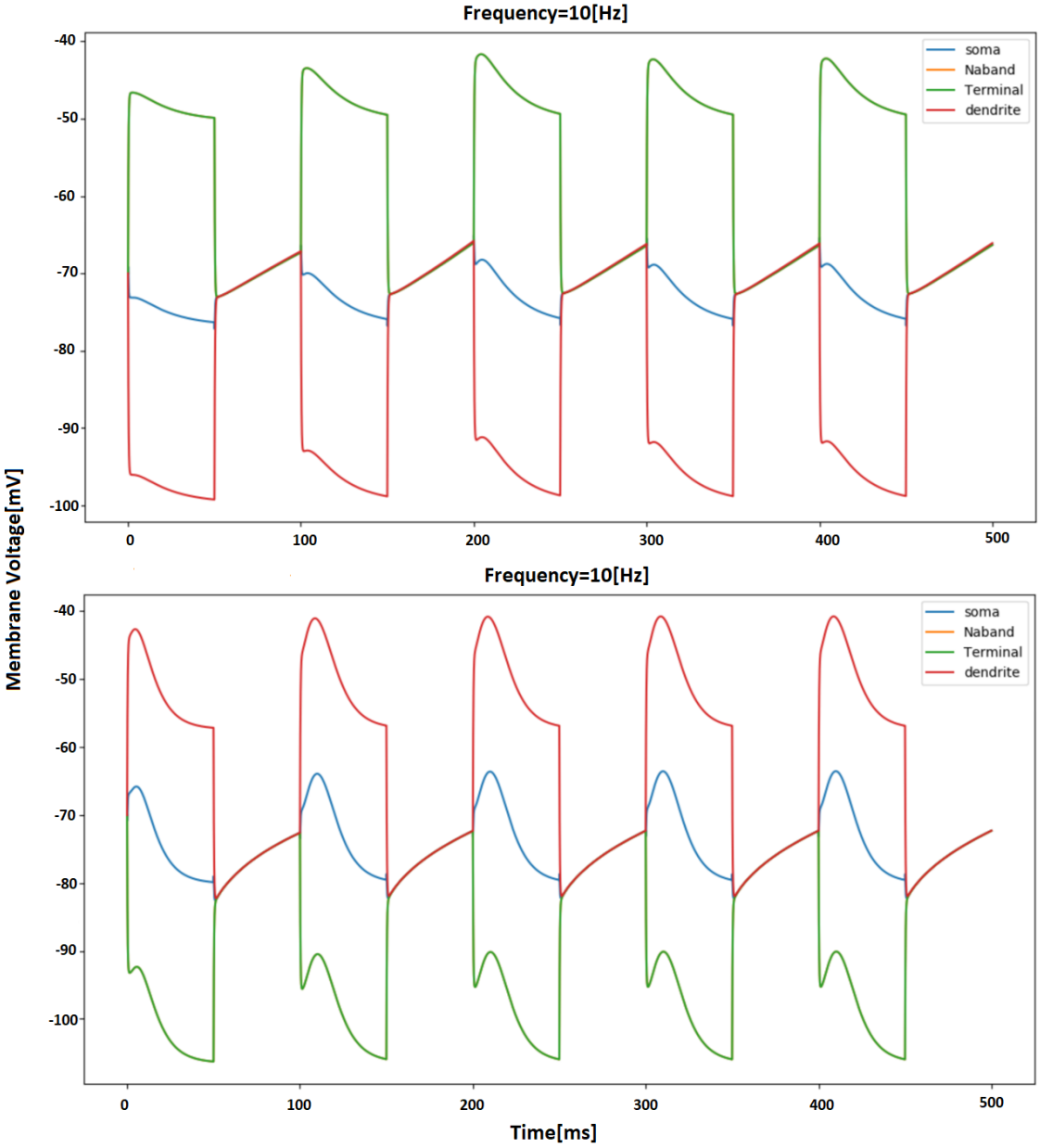

Figure 4.20: Upper case $5\mu A$ external current amplitude in frequency 10 Hz, lower case: $-5\mu A$ external current amplitude in frequency 10 Hz. In the second half of each period, soma and dendrite are coincident while sodium band and terminal are entirely coincident.

- **Anodic and cathodic rectangular pulses with the amplitude** $5\mu A$

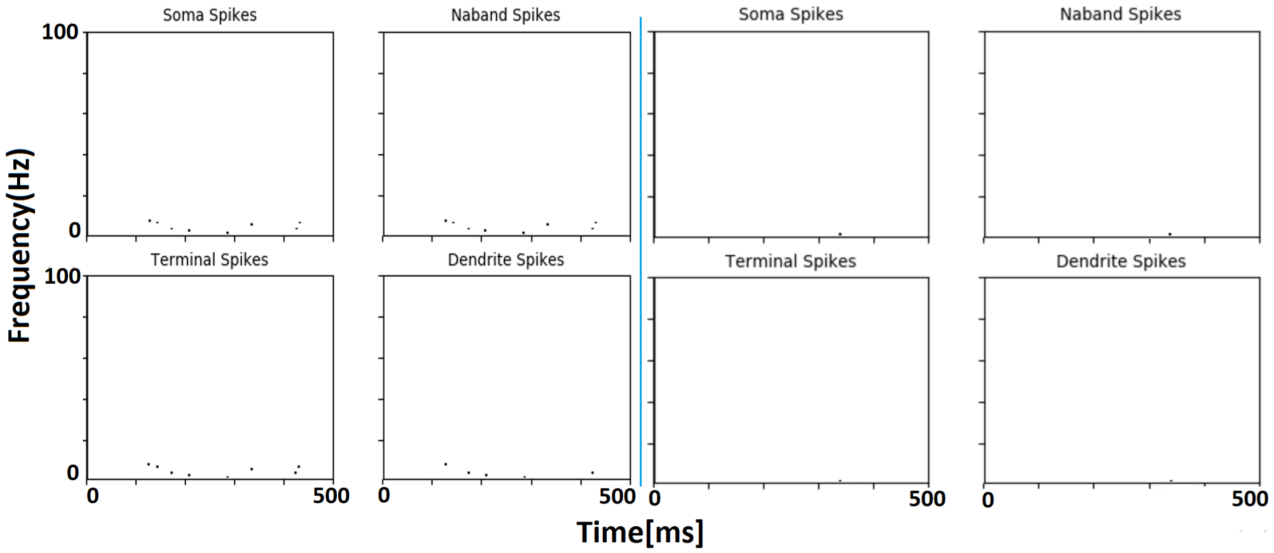

Figure 4.21: Left: $+5\mu A$, same amplitude of anodic pulses produces more APs. Due to the low amplitude of APs at dendrite, a few number of APs are recorded compared to the other three regions. Right: $-5\mu A$, low amplitude of extracellular stimulation current results in just one AP in case of cathodic pulses.

- **Anodic and cathodic rectangular pulses with the amplitude** $6\mu A$

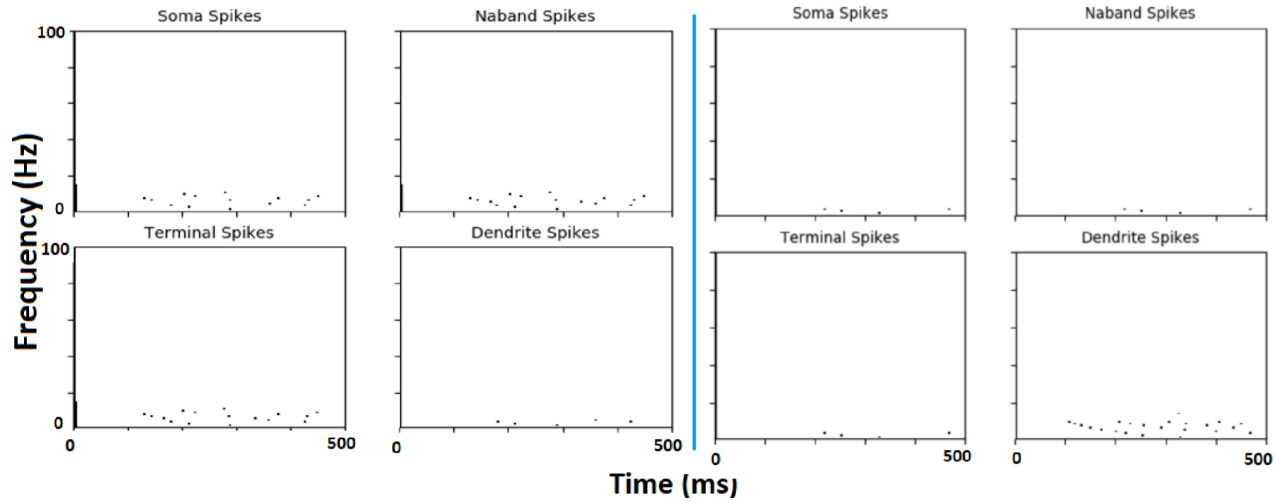

Figure 4.22: left: $+6\mu A$, In case of anodic pulses, more APs are produced at the three regions: sodium band, soma and terminals. Some APs at dendrite may not have been recorded due to their amplitudes are below the defined amplitude. Right: $-6\mu A$, however, at dendrite, more spikelets are produced with cathodic pulses.

- **Anodic and cathodic rectangular pulses with the amplitude** $7\mu A$

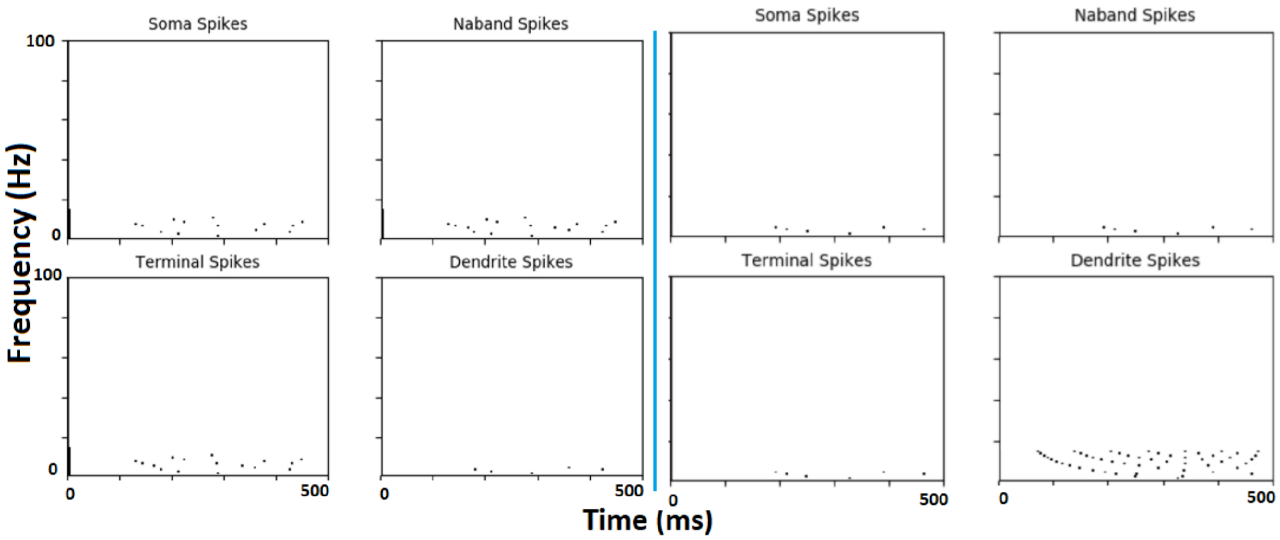

Figure 4.23: Left: $+7\mu A$, in case of anodic pulses, more APs are produced at the three regions: sodium band, soma and terminals. Due to the low amplitude of APs at dendrite, a few number of APs are recorded compared to the other three regions. Right: $-7\mu A$, however, at dendrite, more spikelets are produced with cathodic pulses.

4.2.1 Summary

An anodic pulse can produce more APs compared to its corresponding cathodic pulse, except at dendrites which are generating more spikelets rather than APs. When the polarity of the stimulus is changed from anodic to cathodic, most hyperpolarised dendrite become the most depolarised part of the cell and reach the amplitude of -40 mV which is the defined threshold for the dendritic spikelet in this study, therefore, in case of cathodic pulses, more spikelets are recorded at dendrite. Additionally, all figures show that higher amplitudes are needed to produce action potentials. However, as mentioned before this study investigates the ability of the cell to produce AP and not spikelet. Therefore if the defined threshold is considered lower, there might be more reaction of the cell since the BCs work via graded potential rather than action potential. Moreover, as demonstrated above further investigation needs to be done with different amplitudes to analyse the reaction of the cell to extracellular stimulation.

4.3 Noise

A possible approach to understanding the neuronal bases of the computational properties of the neural networks consists of modelling its basic building blocks, neurons and synapses, and then simulating their collective activity emerging in large networks. In developing such models, a satisfactory description level must be chosen as a compromise between simplicity and faithfulness in reproducing experimental data. Deterministic neuron models (i.e., models that upon repeated simulation with fixed parameter values provide the same results) are usually made up of ordinary differential equations and allow for relatively fast simulation times. By contrast, they do not describe accurately the underlying stochastic response properties arising from the microscopical correlate of neuronal excitability. Stochastic models are usually based on mathematical descriptions of individual ion channels, or on an effective macroscopic account of their random opening and closing.

In this contribution, a channel noise is added to the simulation to compute more realistic responses. This term was presented previously [Rattay et al.(2001)], and the noise was assumed to be directly proportional to the sodium channel density ($g_{Nav1.1}$) at each compartment where I_{noise} changed its value every step (0.01 ms)

$$I_{noise,n} = rand \times k_{noise} \times (g_{Na} \times A_n)^{1/2} \tag{4.3}$$

With rand representing Gaussian (0, 1). In the following sections, it has been attempted to find an appropriate k_{noise} for the DB4 cell. Therefore, every step is clearly explained and demonstrates the results of different k values. In the end, some stimulations will be repeated with the noise to compare the results.

4.3.1 How to obtain a suitable noise factor

Neurons can generate oscillatory activities, caused by mechanisms within individual neuron or even this can be found in a neural network by the interaction between neurons. In individual neurons, these oscillations appear either as some in membrane potentials or even as patterns of APs which result in synaptic activities. Neural oscillations were observed by Hans Berger in 1924, but the origin of this is still not understood. The intensity of these activities is very dependent on the cell type. Some cells such as GCs are more sensitive. Therefore they have more spontaneous activities and APs in the absence of stimulus in contrast to the BCs.
In order to find a proper k_{noise}, a noise contribution simulation of the cell without any stimulus has been run for different values of k_{noise}. The spontaneous activities are observed and compared to find the most suitable k_{noise} value. To compare the spontaneous activities, the Root Mean Square (RMS) of the membrane voltage is calculated. The RMS value of a set a continuous-time waveform is the square root of the arithmetic mean of the squares of the values, or the square of the function that defines the continuous waveform.

In the case of a set of n values $x_1, x_2, x_3., x_n$

$$RMS = \sqrt{\frac{1}{n} \times (x_1^2 + x_2^2 + \ + x_n^2)} \tag{4.4}$$

A wide range of k_{noise} values was run 20 times for 500 ms, in $k_{noise} = 0.016 \frac{\mu A}{(mS)^{1/2}}$ the first spontaneous AP was observed, therefore this value can be a critical value as shown in Figure 4.24 and the RMS amplitudes need to be calculated. This value in all four regions are: In soma 10.351 mV, in sodium band 11.921 mV, in terminal 11.865 mV and dendrite 10.113 mV.

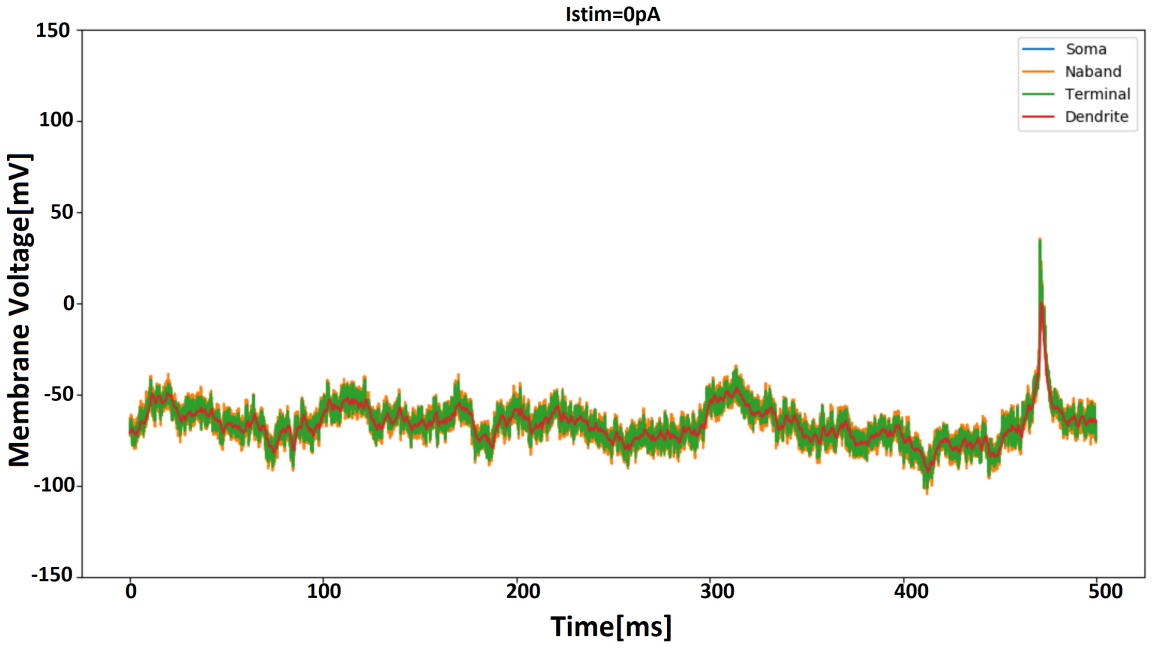

Figure 4.24: $k_{noise} = 0.016 \frac{\mu A}{(mS)^{1/2}}$

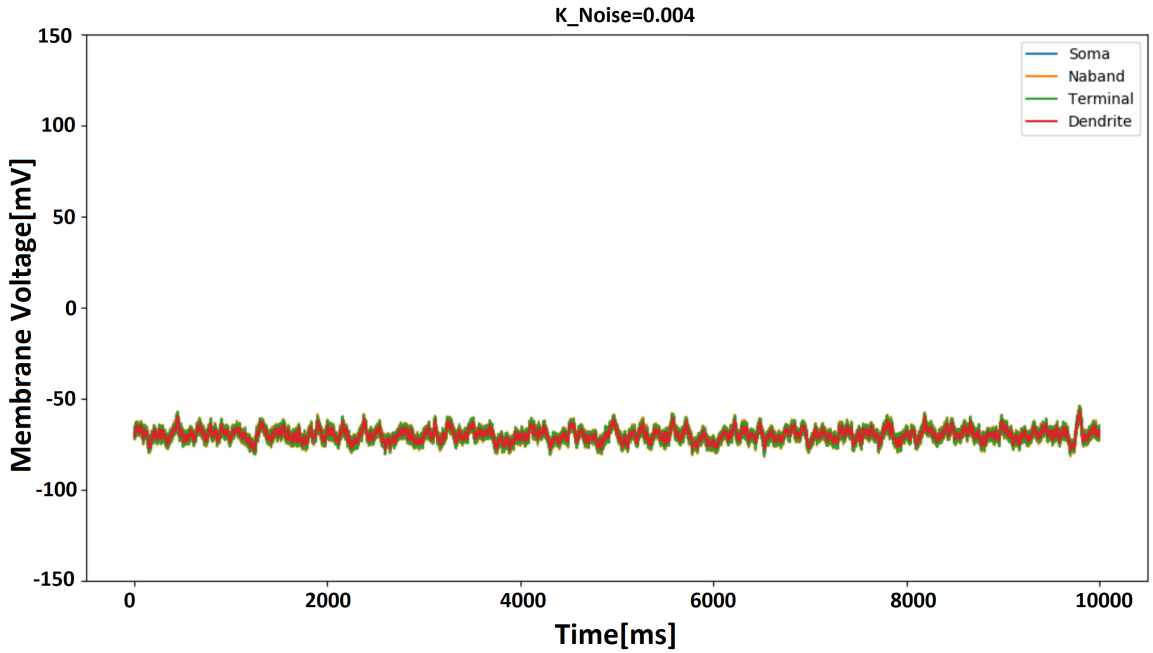

Figure 4.25: $k_{noise} = 0.004 \frac{\mu A}{(mS)^{1/2}}$

In contrast to the typical values in investigations such as in [Rattay et al.(1999)], these values

are substantial. Hence 0.016 cannot be a suitable choice, and a decidedly smaller k_{noise} needs to be found. Therefore $k_{noise} = 0.004\frac{A}{(mS)^{1/2}}$ has been chosen and investigated, this was run for 10 s which is about 20 times longer than previous recording times. But no AP was observed and might need even hours to generate an AP. The RMS values were calculated: In soma 3.131 mV, in sodium band 3.353 mV, in terminal 3.328 mV and dendrite 3.109 mV. These values are still larger than normal values which have been found for $k_{noise} = 0.001\mu A/(mS)^{1/2}$ with RMS amplitude in soma 0.803 mV, in sodium band 0.870 mV, in terminal 0.8667 mV and dendrite 0.793 mV.

4.4 Simulations with noise

Adding noise to the simulations lead to different results in repetitive runs with even always same parameters. Therefore, it should be a way to compare this function. However, this could be done by computing a probability for spiking at different amplitudes. This curve is plotted by steady increasing stimulus amplitude and repeat the experiment for multiple times for instance here each amplitude was repeated for 20 times then the probability was computed for each current amplitude. The stimulus was a single rectangular pulse which was driven for 0.1 of the whole runtime. In order to compare and find a proper value of the k_{noise}, a sigmoid function (Boltzmann equation [Tsai et.al(2009)]) is used.

$$spike\ probability(I) = \frac{100}{1 + exp(-(I - a)/b)} \tag{4.5}$$

Parameter a is the amplitude near the 50% spiking probability. Parameter b is the slope of the sigmoid curve to fit the curve to the computed data. As shown in Figure 4.21 three dierent sigmoid curves for the As shown in Figure 4.26 three different sigmoid curves for the $k_{noise} = 0.001, 0.004$, and $0.016\mu A/(mS)^{1/2}$, respectively.

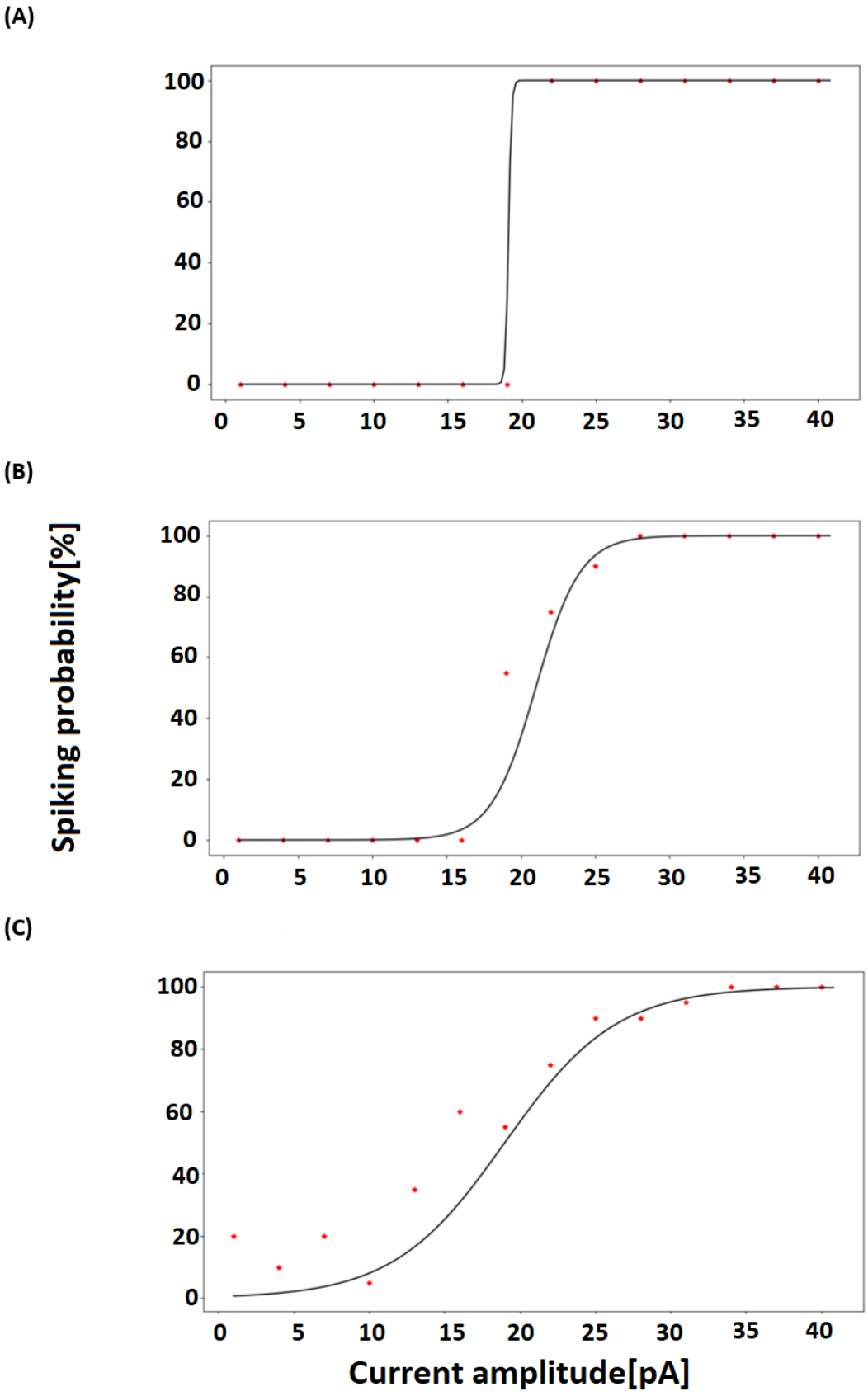

Figure 4.26: (A): $k_{noise} = 0.001\mu A/(mS)^{1/2}, (B) : k_{noise} = 0.004\mu A/(mS)^{1/2}, (C) : k_{noise} = 0.016\mu A/(mS)^{1/2}$

The RMS values calculated from the previous section shows that the most acceptable value for the k_{noise} is 0.001, which is shown that the cell will not act stochastically. This again shows the nature of the bipolar cells. Since BCs are not sensitive cells such as pyramid cells or Ganglion cells, they will not have spontaneous activities as likely as GCs.

Due to having a possible corresponding to the reality, some stimulations from section 3.1 are repeated to compare a condition closer to the real situations with computer simulations. For this purpose the $k_{noise} = 0.004\mu A/(mS)^{1/2}$ was chosen. This value still might not have reliable RMS values but it is not as unusual as the RMS values of $k_{noise} = 0.016\mu A/(mS)^{1/2}$ therefore, it could be fair enough for this comparison.

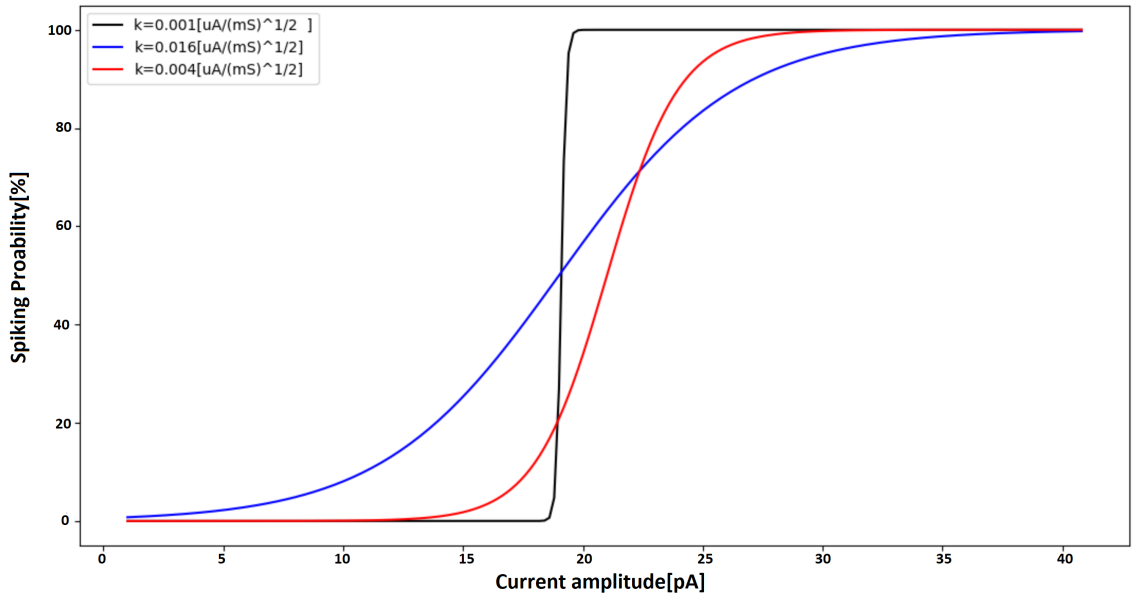

Figure 4.27: Comparison of three different k_{noise} value of 0.001, 0.016 and 0.004 $\mu A/(mS)^{1/2}$

- **Anodic rectangular pulses with the amplitude of 20 pA**

  This amplitude may not be enough to stimulate the cell. However, in contrast to Figure 4.5, the cell has responded with more APs with a stochastic pattern.

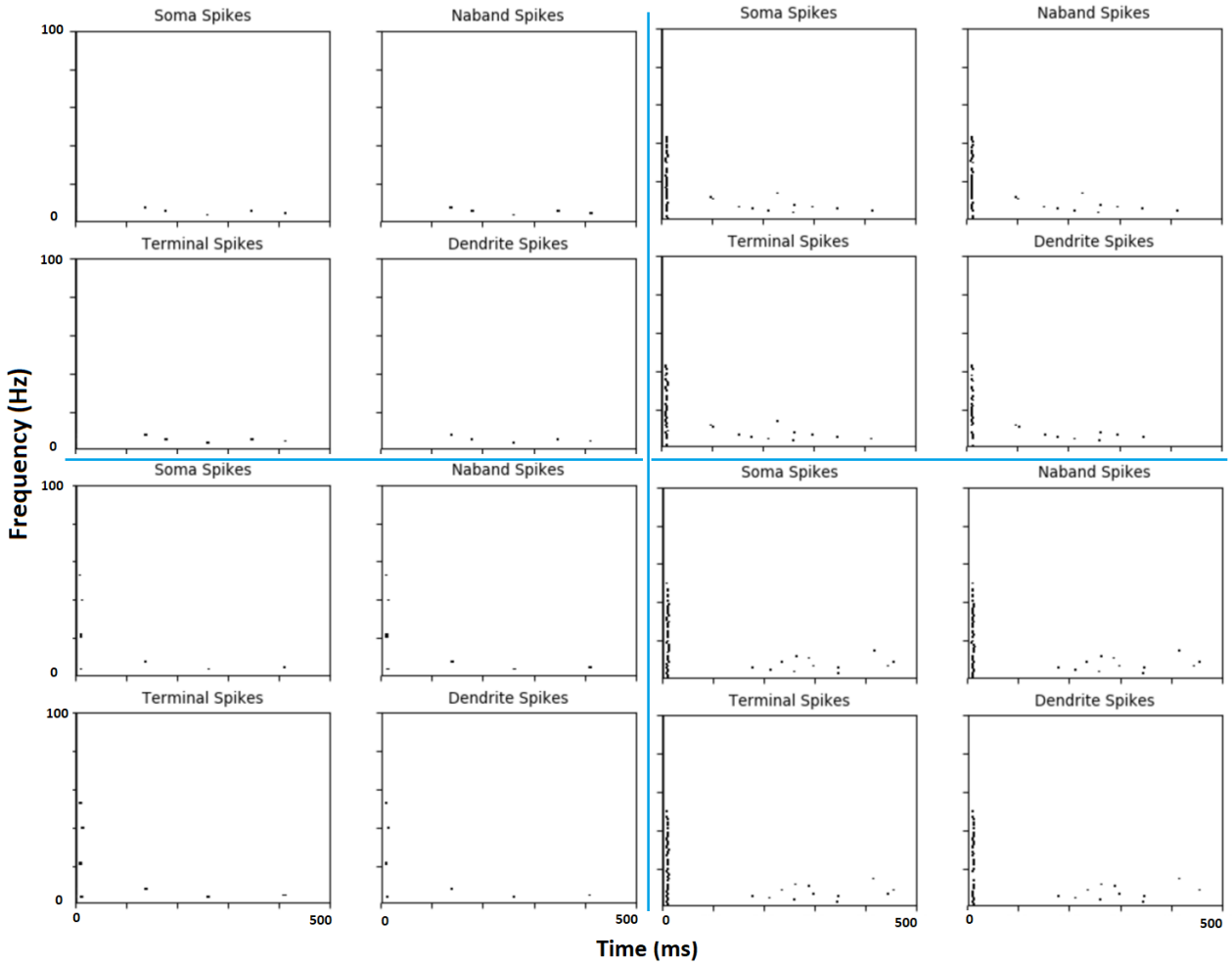

Figure 4.28: Top left: injection in dendrite, Top right: injection in sodium band, Bottom right: injection in terminal, Bottom left: injection in soma

- **Anodic rectangular pulses with the amplitude of 30 pA**

  In contrast to Figure 4.7, more APs with more stochastic pattern have happened especially In dendrite and terminal.

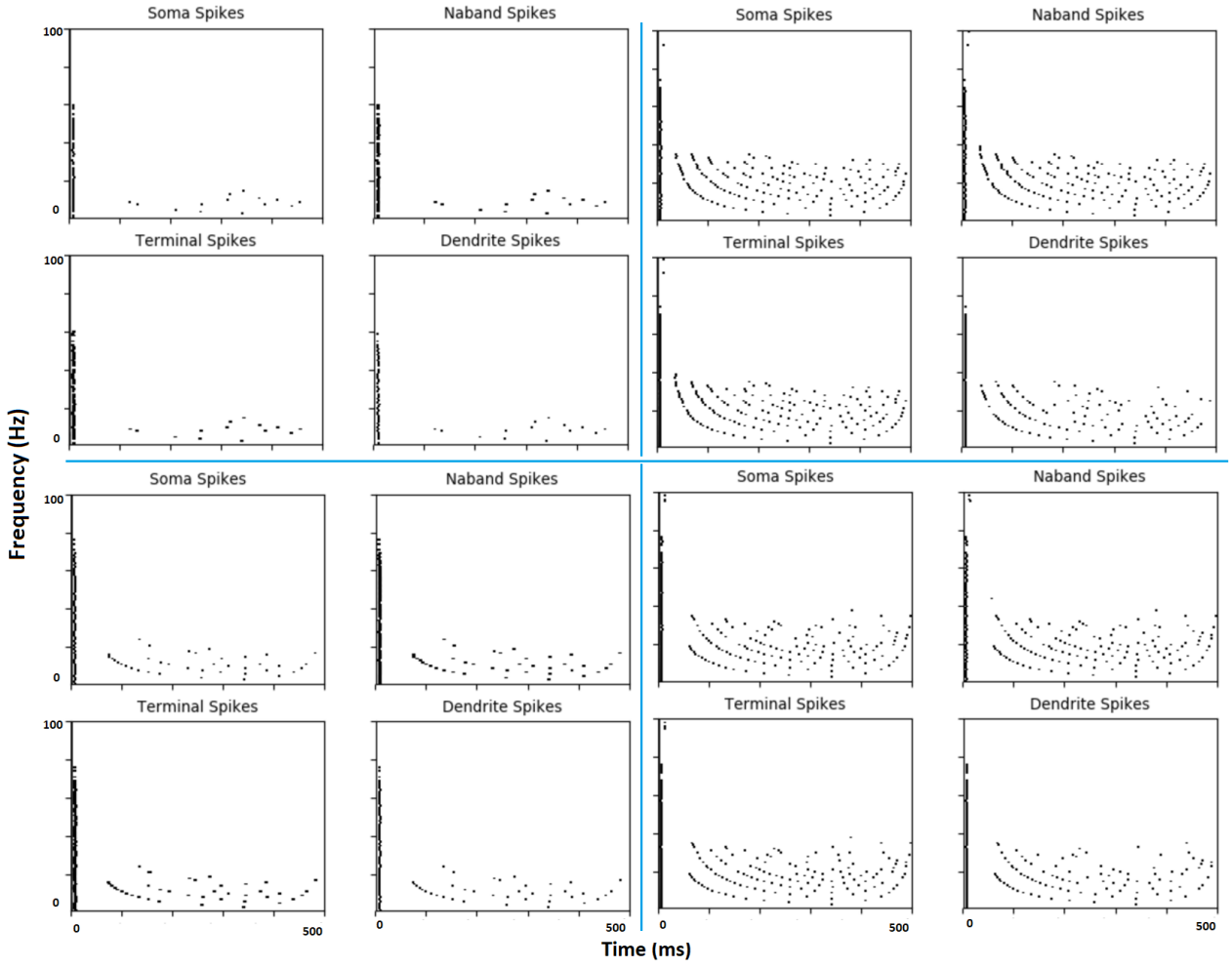

Figure 4.29: Top left: injection in dendrite, Top right: injection in sodium band, Bottom right: injection in terminal, Bottom left: injection in soma

- **Anodic sinusoidal pulses with the amplitude of 30 pA**

  30 pA is not a suitable amplitude of the sinusoidal pulse as demonstrated before. However, after adding the noise channel, in some cases may more than one AP has occurred and the cell has responded in higher frequencies such as 100 Hz which has happened with the presence of the noise.

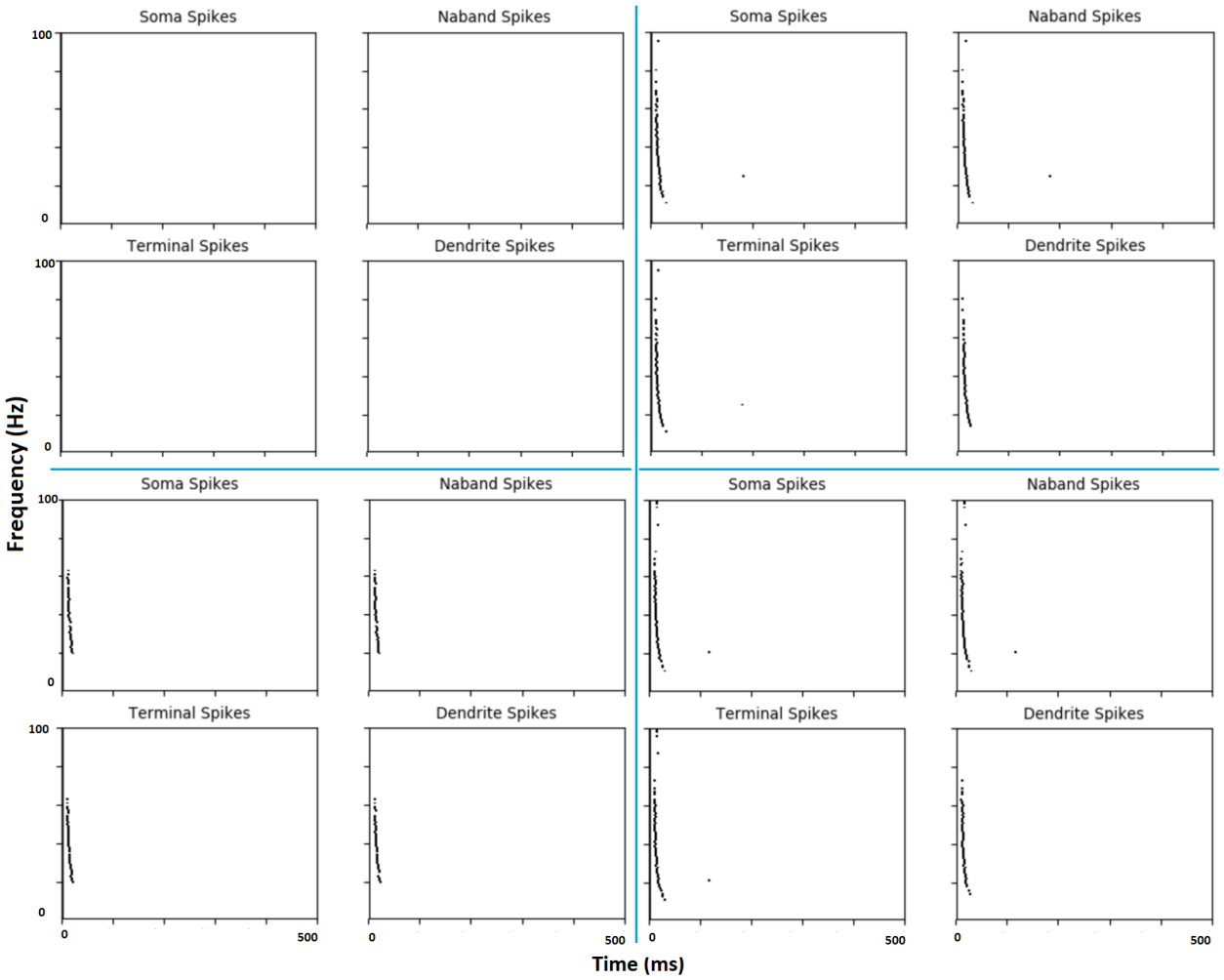

Figure 4.30: Top left: injection in dendrite, Top right: injection in sodium band, Bottom right: injection in terminal, Bottom left: injection in soma

- **Anodic sinusoidal pulses with amplitude of 50 pA**

  Figure 4.31 demonstrates that An amplitude of 50 pA causes more stochastic patterns of APs in contrast to the absence of the noise with the similar sinusoidal extracellular stimulation.

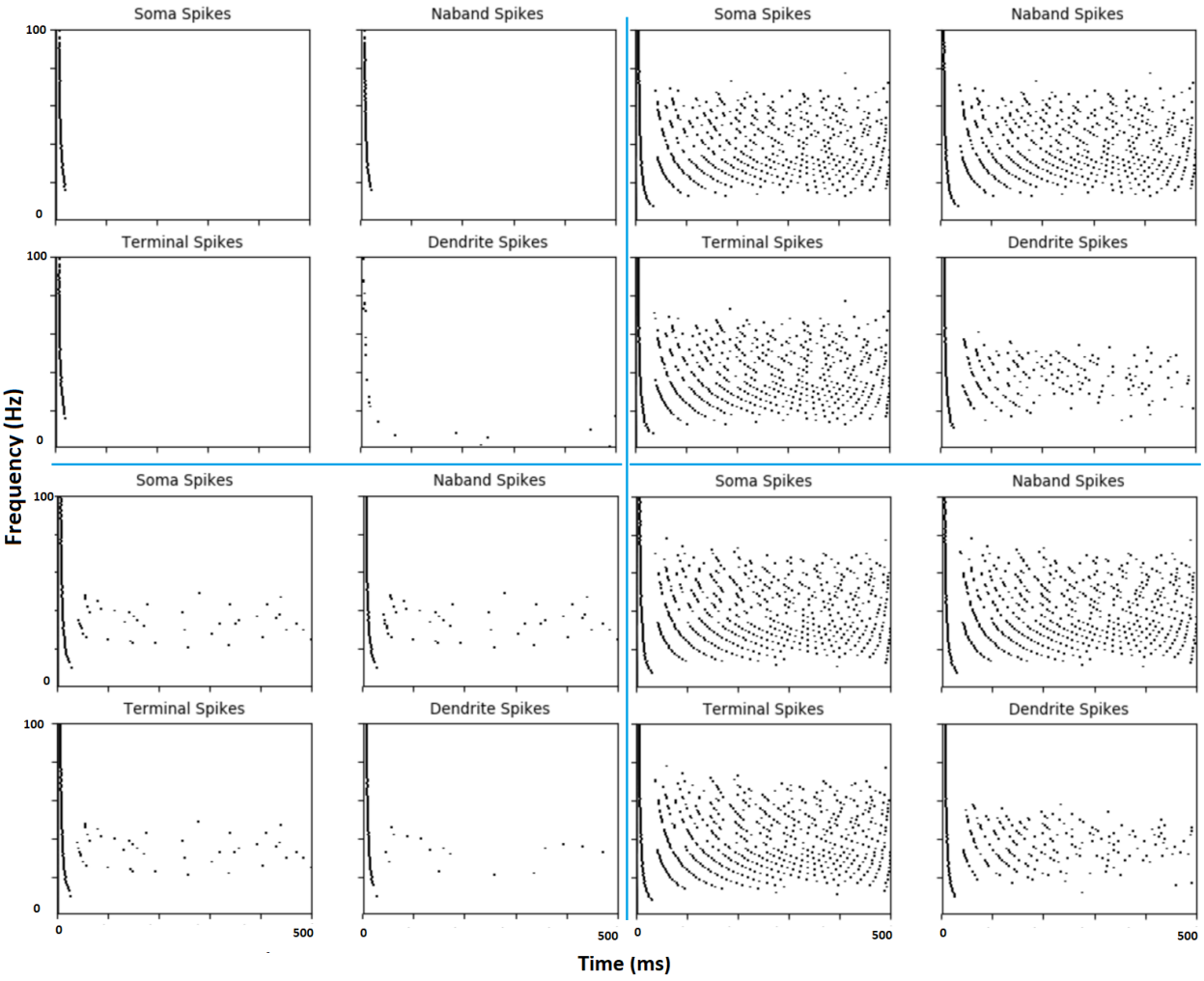

Figure 4.31: Top left: injection in dendrite, Top right: injection in sodium band, Bottom right: injection in terminal, Bottom left: injection in soma

4.4.1 Summary

The noise contribution causes a stochastic arrangement of APs as shown in the raster plots. However, because of the less sensitive nature of BCs, higher k_{noise} is not suitable for this cell. Therefore, stochastic behaviour of the cell may not be appreciably observable in some cases. The figures demonstrate that noise does not always cause more APs, but in some cases, it even inhibits the occurrence of APs. For instance, comparing corresponding figures before and after noise contribution (Figure 4.12 and Figure 4.29 or Figure 4.15 and Figure 4.31), in case of sodium band and terminal injection some APs are inhibited while in case of soma and dendrite injection more APs are produced, and the noise has amplified the stimulus.

Chapter 5

Discussion and Conclusion

In summary, in this study, a single DB4 is simulated, and the simulation process has been demonstrated in detail to give some knowledge for further computational purposes. Then, the cell was stimulated through intra and extracellular electrical stimulation. The stimulation time was 500 ms in all cases via a periodic pulse within a frequency range of 1 to 100 Hz; the cell response has been recorded in four regions of the cell. At the end of the Result chapter, a noise channel has been added to the simulations to mimic an experimental condition due to comparing with the previous conditions.

Regarding intracellular stimulation, 20 pA rectangular pulses have been considered as the critical amplitude regarding that the electrode position was essential and cell did not respond when the electrode was set at neither dendrite nor terminals. However, the cell's responses showed that more energy is needed. At 25 pA of amplitude, cell responded with more APs, some APs has appeared in terminal site, but there was no AP at dendrite site until the amplitude of 30 pA. The cell's responses displayed that DB4 needs higher amplitudes and even more energy at dendrite site. The reason might be due to the nature of bipolar cells which are less sensitive than the other cell types such as GCs. At high amplitudes of rectangular stimulus with injection at soma and sodium bands, the frequency range for high excitation was between

20 to 80 Hz which is broader than the frequency range of sinusoidal pulses. In case of sinusoidal stimulus, higher amplitudes are needed to get a similar response with the rectangular pulse

Regarding the extracellular stimulation, the response of the cell was more on a scale of spikelets rather than APs. However, since this study investigates the APs, the spikelets are not taken into account. Thus, in the range of amplitude from 5 to 7 μA, just a few numbers of APs have appeared. An important fact demonstrated in the results is that in the case of an anodic stimulus more APs are produced compared to the cathodic stimulus with the same amplitude. However more investigation is needed to find an adequate range of amplitude to stimulate the cell with more APs.

At the final section, a noise channel has been added to the simulations. The associated noise stimulations showed more irregular and stochastic cell responses. However, the cell needs larger values of k_{noise} to show more stochastic behaviour. On the other hand, by increasing k_{noise}, RMS values becomes substantial and unacceptable. The two contradictory facts show that the cell is not a sensitive cell and it does not have spontaneous activities as much as sensitive cells do. Therefore, for further investigations, a more sensitive cell is required to contrast the noise influence on computer simulations, and this cell may not be a suitable case for this purpose.

Bibliography

Abbott, Larry F. "Lapicques introduction of the integrate-and-fire model neuron (1907)." Brain research bulletin 50.5-6 (1999): 303-304.

Aradi, Ildiko, and Ivan Soltesz. "Modulation of network behaviour by changes in variance in interneuronal properties." The Journal of physiology 538.1 (2002): 227-251.

Barela, Arthur J., et al. "An epilepsy mutation in the sodium channel SCN1A that decreases channel excitability." Journal of Neuroscience 26.10 (2006): 2714-2723.

Barnes, Nick, et al. "Vision function testing for a suprachoroidal retinal prosthesis: effects of image filtering." Journal of neural engineering 13.3 (2016): 036013.

Barriga-Rivera, Alejandro, et al. "Visual Prosthesis: Interfacing Stimulating Electrodes with Retinal Neurons to Restore Vision." Frontiers in neuroscience 11 (2017): 620.

Blakeslee, Barbara, and Mark E. McCourt. "What visual illusions tell us about underlying neural mechanisms and observer strategies for tackling the inverse problem of achromatic perception." Frontiers in human neuroscience 9 (2015): 205.

Boycott, Brian Blundell, and John Elliott Dowling. "Organization of the primate retina: Light microscopy, with an appendix: A second type of midget bipolar cell in the primate retina." Phil. Trans. R. Soc. Lond. B 255.799 (1969): 109-184.

Byrne John H. Chapter 2 - Intracellular Stimulation, Electrical Stimulation Research Techniques, Academic Press (1981): Pages 37-59.

Cavallo, Tiberius. "VI. An account of some new electrical experiments." Philosophical Transactions of the Royal Society of London 67 (1777): 48-55.

Chader, Gerald J., and Michael Young. "Preface: Sight restoration through stem cell therapy." Investigative ophthalmology & visual science 57.5 (2016): ORSFa1-ORSFa5.

da Cruz, Lyndon, et al. "Five-year safety and performance results from the Argus II retinal prosthesis system clinical trial." Ophthalmology 123.10 (2016): 2248-2254.

Deleuze, Charlotte, et al. "T-type calcium channels consolidate tonic action potential output of thalamic neurons to neocortex." Journal of Neuroscience 32.35 (2012): 12228-12236.

Department of Neurobiology and Anatomy, McGovern Medical School, University of Texas. Chapter 14: Visual Processing: Eye and Retina Valentin Dragoi,2000

Duncan, Jacque L., et al. "Improvements in visionrelated quality of life in blind patients implanted with the Argus II Epiretinal Prosthesis." Clinical and Experimental Optometry 100.2 (2017): 144-150.

Foerster, O. "Beitrage zur Pathophysiologie der Sehbahn und der Sehsphare." J. Psychol. Neurol., Lpz. 39 (1929): 463.

Fried, Shelley I., et al. "Axonal sodium-channel bands shape the response to electric stimulation in retinal ganglion cells." Journal of neurophysiology 101.4 (2009): 1972-1987.

Garcia, Liliana, et al. "High-frequency stimulation in Parkinson's disease: more or less?." Trends in neurosciences 28.4 (2005): 209-216.

Gear, C. William. Numerical initial value problems in ordinary differential equations. Prentice Hall PTR, 1971.

Husser, Michael, Nelson Spruston, and Greg J. Stuart. "Diversity and dynamics of dendritic signaling." Science 290.5492 (2000): 739-744.

Hodgkin, Allan L., and Andrew F. Huxley. "The components of membrane conductance in the giant axon of Loligo." The Journal of physiology 116.4 (1952a): 473-496.

Hodgkin, Alan L., and Andrew F. Huxley. "A quantitative description of membrane current and its application to conduction and excitation in nerve." The Journal of physiology 117.4 (1952b): 500-544.

Hu, Wenqin, et al. "Distinct contributions of Na v 1.6 and Na v 1.2 in action potential initiation and backpropagation." Nature neuroscience 12.8 (2009): 996.

Isaacson, Walter. Benjamin Franklin: An American Life. Simon and Schuster, 2003.

Jeng, J., et al. "The sodium channel band shapes the response to electric stimulation in retinal ganglion cells." Journal of neural engineering 8.3 (2011): 036022.

Kandel, E. R. "Sensory experience and the fine-tuning of synaptic connections." Principles of neural science (2000).

Koch, Christof, and Idan Segev, eds. Methods in neuronal modeling: from ions to networks. MIT press, 1998.

Kolb, Helga, Ralph Nelson, and Andrew Mariani. "Amacrine cells, bipolar cells and ganglion cells of the cat retina: a Golgi study." Vision research 21.7 (1981): 1081-1114.

Lane, Frank John, et al. "Perspectives of optic nerve prostheses." Disability and Rehabilitation: Assistive Technology 11.4 (2016): 301-309.

LeRoy, C. "O l'on rend compte de quelques tentatives que l'on a faites pour gurir plusieurs maladies par l'lectricit." Hist Acad Roy Sciences Memoires Math Phys 60 (1755): 87-95.

Lewis, Philip M., and Jeffrey V. Rosenfeld. "Electrical stimulation of the brain and the development of cortical visual prostheses: an historical perspective." Brain research 1630 (2016): 208-224.

Ling, G., and R. W. Gerard. "The normal membrane potential of frog sartorius fibers." Journal of cellular and comparative physiology 34.3 (1949): 383-396.

Mainen, Zachary F., and Terrence J. Sejnowski. "Influence of dendritic structure on firing pattern in model neocortical neurons." Nature 382.6589 (1996): 363.

Masland, Richard H. "The tasks of amacrine cells." Visual neuroscience 29.1 (2012): 3-9.

McNeal, D. R. "Analysis of a model for excitation of myelinated nerve." IEEE Trans. Biomed. Eng. 33 (1986): 974-977.

Merabet, Lotfi B., et al. "What blindness can tell us about seeing again: merging neuroplasticity and neuroprostheses." Nature Reviews Neuroscience 6.1 (2005): 71.

Nguyen, Hieu T., et al. "Thalamic visual prosthesis." IEEE Transactions on Biomedical Engineering 63.8 (2016): 1573-1580.

Osterberg, G. A. "Topography of the layer of the rods and cones in the human retima." Acta ophthalmol 13.6 (1935): 1-102.

Palmer, Lucy M., and Greg J. Stuart. "Membrane potential changes in dendritic spines during action potentials and synaptic input." Journal of Neuroscience 29.21 (2009): 6897-6903.

Polyak. S. L . The Retina. The University of Chicago Press (1941), Chicago.

Prochazka, Arthur, Vivian K. Mushahwar, and Douglas B. McCreery. "Neural prostheses." The Journal of physiology 533.1 (2001): 99-109.

Protti, Dario A., and Isabel Llano. "Calcium currents and calcium signaling in rod bipolar cells of rat retinal slices." Journal of Neuroscience 18.10 (1998): 3715-3724.

Purves, Dale, et al. Cognitive Neuroscience. Sunderland: Sinauer Associates, Inc, 2008.

Puthussery, Theresa, et al. "NaV1. 1 channels in axon initial segments of bipolar cells augment input to magnocellular visual pathways in the primate retina." Journal of Neuroscience 33.41 (2013): 16045-16059.

Ramsden, Conor M., et al. "Stem cells in retinal regeneration: past, present and future." Development 140.12 (2013): 2576-2585.

Rattay, Frank. "On the upper threshold phenomenon of extracellular neural stimulation." Journal of neurophysiology 112.10 (2014): 2664-2665.

Rattay, Frank, Hassan Bassereh, and Andreas Fellner. "Impact of Electrode Position on the Elicitation of Sodium Spikes in Retinal Bipolar Cells." Scientific reports 7.1 (2017): 17590.

Rattay, Frank, Robert J. Greenberg, and Susanne Resatz. "Neuron modeling." Handbook of Neuroprosthetic Methods (2002): 39-71.

Rattay, Frank, Petra Lutter, and Heidi Felix. "A model of the electrically excited human cochlear neuron: I. Contribution of neural substructures to the generation and propagation of spikes." Hearing research 153.1-2 (2001): 43-63.

Rattay, F., L. P. Paredes, and R. N. Leao. "Strengthduration relationship for intra-versus extracellular stimulation with microelectrodes." Neuroscience 214 (2012): 1-13.

Rattay, Frank. "The basic mechanism for the electrical stimulation of the nervous system." Neuroscience 89.2 (1999): 335-346.

Sheasby, Brent W., and Jurgen F. Fohlmeister. "Impulse encoding across the dendritic morphologies of retinal ganglion cells." Journal of neurophysiology 81.4 (1999): 1685-1698.

Shepherd, Robert K., et al. "Visual prostheses for the blind." Trends in biotechnology 31.10 (2013): 562-571.

Soto, Florentina, et al. "Coordinated increase in inhibitory and excitatory synapses onto retinal ganglion cells during development." Neural development 6.1 (2011): 31.

Spampanato, Jay, et al. "Increased neuronal firing in computer simulations of sodium channel mutations that cause generalized epilepsy with febrile seizures plus." Journal of neurophysiology 91.5 (2004): 2040-2050.

Sterratt, David, et al. Principles of computational modelling in neuroscience. Cambridge University Press, 2011.

Stingl, Katarina, et al. "Subretinal visual implant alpha IMSclinical trial interim report." Vision research 111 (2015): 149-160.

Stoer, Josef, and Roland Bulirsch. Introduction to numerical analysis. Vol. 12. Springer Science & Business Media, 2013.

Tsai, David, et al. "Direct activation and temporal response properties of rabbit retinal ganglion cells following subretinal stimulation." Journal of neurophysiology 102.5 (2009): 2982-2993.

Tsukamoto, Yoshihiko, and Naoko Omi. "OFF bipolar cells in macaque retina: type-specific connectivity in the outer and inner synaptic layers." Frontiers in neuroanatomy 9 (2015): 122.

Weiland, James D., Wentai Liu, and Mark S. Humayun. "Retinal prosthesis." Annu. Rev. Biomed. Eng. 7 (2005): 361-401.

Werginz, Paul, and Frank Rattay. "The impact of calcium current reversal on neurotransmitter release in the electrically stimulated retina." Journal of neural engineering 13.4 (2016): 046013.

Zeng, Fan-Gang, et al. "Cochlear implants: system design, integration, and evaluation." IEEE reviews in biomedical engineering 1 (2008): 115-142.

Zhang, H., et al. "Mathematical models of action potentials in the periphery and center of the rabbit sinoatrial node." American Journal of Physiology-Heart and Circulatory Physiology 279.1 (2000): H397-H421.